The Dissertation Committee for Harshal Dilip Gupta
certifies that this is the approved version of the following dissertation:

Negative Molecular Ions in the Laboratory and in Space

Committee:

John F. Stanton, Supervisor

Patrick Thaddeus, Supervisor

Michael C. McCarthy

Neal J. Evans II

Jason B. Shear

David A. Vanden Bout

Negative Molecular Ions in the Laboratory and in Space

by

Harshal Dilip Gupta, B.S.

DISSERTATION

Presented to the Faculty of the Graduate School of

The University of Texas at Austin

in Partial Fulfillment

of the Requirements

for the Degree of

DOCTOR OF PHILOSOPHY

THE UNIVERSITY OF TEXAS AT AUSTIN

December 2009

"One's ideas must be as broad as Nature if they are to interpret Nature."

– Sherlock Holmes

"Let us adopt an attitude of revolutionary optimism."

– Patrick Thaddeus

Acknowledgments

It is a great pleasure to acknowledge the many colleagues and friends who have made my long journey through graduate school enjoyable and fulfilling. Their considerable support and presence over the past six years has enriched my life, enabling me to perform at my best and to finally arrive at this important milestone.

First and foremost I thank my thesis advisors—John Stanton and Patrick Thaddeus—the two men who have had the most influence on my growth as a scientist. John Stanton has been an exemplary teacher, advisor, friend, and above all a kind and compassionate human being. He welcomed me into his group as a graduate student, even though my interests went beyond theoretical chemical physics. Far from merely tolerating my interest in experimental work and astronomy, he supported and encouraged it whole-heartedly, both intellectually and financially, allowing me great freedom in the research I wanted to pursue. Nothing I can possibly say will ever fully express my gratitude for John's presence in my life: for his unwavering support and tremendous mentorship, I am forever in his debt. It is through John that I was introduced to Patrick Thaddeus and his laboratory at Harvard, where my research found a focus and culminated in this thesis.

Pat Thaddeus has been a great mentor during the past four years,

providing the ideas as well as the resources which have enabled me to do this work. His focus on and enthusiasm for the work on molecular anions have been inspiring. His precision of thought and clarity of exposition are qualities that I seek to emulate throughout my life. I cannot recall a single dull moment in the nearly four years I spent in Pat's group. Our meetings at the "white table" often brightened my days, as it was there that I heard Pat's anecdotes—of which there is an abundant supply. Often, when we appeared to have hit a wall in our laboratory searches, he would give us "pep talks". The quotation that forms half the dedication for this thesis was intended to lift our spirits perforce after our second search for C_3N^- had failed—we found the molecule on the very next attempt! It has been my exceedingly good fortune to have learned from Pat, and I shall always value his advice, especially on writing and speaking, and strive to be better at both. By the time this thesis reaches you, it will undoubtedly have been smoothed under his kind and critical eye.

Second, I thank my senior colleagues in the spectroscopy lab at Harvard: Michael McCarthy and Carl Gottlieb, for teaching me much of what I know about laboratory spectroscopy and radio astronomy. Mike and Carl are two of the most able and critical scientists I know, and it has been a pleasure and an honor learning from them. I would also like to thank Sandra Brünken, who was a post-doc in the Thaddeus group, and an able and kind collaborator—the beautiful work on the astronomical detection of C_8H^- described in this thesis was done in collaboration with her.

Third, I thank the people who helped with the survey of carbon chain

anions and radicals that forms a substantial component of this thesis. I am indebted to Phil Myers at the Center for Astrophysics for many helpful discussions and suggestions during the course of the survey. I am also grateful for helpful suggestions from Tyler Bourke, Sandra Brünken, Neal Evans, Alex Dalgarno, and Bill Klemperer.

Fourth, I acknowledge the colleagues who helped me with some of the calculations that appear in this thesis: Juana Vázquez and Mychel Varner for their help with quantum-chemical calculations, and Michael Harding for helpful discussions on coupled-cluster theory. I am grateful to Elaine Gottlieb for her help with the numerical code for the calculation of partition functions, and to Kelly Higgins for the use of his workstations.

Fifth, I am obliged to the other members of my dissertation committee—Michael McCarthy, Neal Evans, Jason Shear, and David Vanden Bout—for agreeing to serve on my committee, and for their helpful feedback on this dissertation.

Last, but not least, I thank Craig Michoski, Whit Farnum, Harsha Bhat, and Ron Clouse for their friendship, and my family for their love and support.

Negative Molecular Ions in the Laboratory and in Space

Publication No. _____

Harshal Dilip Gupta, Ph.D.
The University of Texas at Austin, 2009

Supervisors: John F. Stanton
Patrick Thaddeus

This dissertation describes the theoretical, laboratory, and astronomical spectroscopy of negative molecular ions (anions), starting with the laboratory detection of the large carbon chain anion C_6H^- in the radio band and its identification in the molecular envelope of the carbon star IRC+10216 and in the cold dark molecular cloud TMC-1. In IRC+10216 the identification solved the long standing problem of the unidentified series of lines with rotational constant 1377 MHz first observed by K. Kawaguchi et al. Rotational spectra of the structurally similar anions—CCH^-, C_4H^-, C_8H^-, CN^-, and C_3N^-—have been detected in the laboratory, and three more anions—C_4H^-, C_8H^-, and C_3N^-—have now been identified in space.

Molecular structure calculations using the CCSD(T) method and large basis sets predicted accurately the rotational constants (B_0) and centrifugal

distortion constants (D_J) of all six anions and their isotopomers, guiding laboratory searches for these species. Reported here are the radio spectra of C_4H^-, C_6H^-, C_8H^-, and C_3N^-, measured to within 0.1 ppm in the centimeter-wave band by Fourier transform microwave spectroscopy of supersonic molecular beams and in the millimeter-wave band by absorption spectroscopy of low-pressure DC discharges. The spectroscopic constants derived from these measurements are so accurate, that the rotational frequencies of the anions can be calculated to within 1 km s^{-1}, adequate for radio searches in essentially all astronomical molecular sources.

Radio astronomical observations with the 100 m Green Bank Telescope (GBT) toward TMC-1 yielded detection of C_8H^-, as well as an improved estimate of the column density of C_6H^-. The two anions are surprisingly abundant relative to their neutral radicals: a C_6H^-/C_6H ratio of 1.6% and a C_8H^-/C_8H ratio of 5% was derived. Upper limits were obtained for C_4H^-/C_4H ($< 0.004\%$) and C_3N^-/C_3N ($< 0.8\%$).

A survey of C_6H^- and the related radicals C_4H and C_6H was done with the GBT toward 24 galactic molecular sources. The C_6H^- ion was newly detected in two dark clouds: L1544 and L1521F; C_4H was detected in nearly all dark clouds surveyed (in six for the first time); and C_6H was newly detected in five dark clouds and a translucent cloud. The observed C_6H^-/C_6H ($1\% - 4\%$) and C_6H/C_4H ($0.2\% - 1\%$) ratios suggest that C_6H^- may be close to detection in many other dark clouds.

Table of Contents

List of Tables

List of Figures

Chapter 1

Introduction

1.1 Background

Negative ions (anions) are important in many areas of chemistry and physics involving weakly ionized gases. The formation of anions can significantly reduce the conductivity of an electrical discharge through an electronegative gas, as they replace the lighter, more mobile electrons as carriers of the negative charge. It is also well known that the loss of free electrons to molecules in the lower layers of the terrestrial ionosphere limits the main regions of the ionosphere capable of reflecting high-frequency radio waves to altitudes above 100 km [1]. After World War II, beams of H^-—the simplest atomic anion—were routinely used to generate low energy protons in particle accelerators [2]. The most striking example, however, of a phenomenon in which negative ions have been shown to play a decisive role is the continuous emission spectrum of the Sun: the absorption by H^- ions present in the solar photosphere essentially determines the spectral energy distribution of the Sun at wavelengths longer than about 5000 Å.

This explanation was first suggested in 1939 by Wildt [3, 4], who proposed that at the temperatures and electron densities in the Sun, a significant

fraction of the hydrogen would be present as H^-, a species with a low electron affinity [1] (0.754 eV) and hence a low threshold for continuous absorption. He showed, using the crude absorption coefficients available at the time, that the fragile H^- could indeed account for the observed absorption—a prediction later confirmed by calculations [5, 6] and a measurement of the photodetachment cross-section of H^- [7]. Wildt's proposal also served to renew interest in negative ions in general[2], which had received little attention since their discovery by Thomson [9] at the beginning of the last century. It is remarkable therefore that in the nearly 70 years since Wildt's demonstration, during which some 130 neutral molecules and 14 positive molecular ions (cations) have been found in space, no molecular anion had been identified.

The presence of molecular anions in the interstellar gas has been considered for more than 30 years. Dalgarno and McCray (1973; [10]) proposed that reactions of negative ions leading to the production of neutral molecules were probably important in dense clouds. In the five years that followed, three carbon chain free radicals—CCH, C_3N and C_4H—unknown in the gas phase in the laboratory, were identified in space by radio astronomy [11–13]. Because these molecules have large electron affinities, it was suggested that they could

[1] The electron affinity, defined as the energy difference between a neutral system and its anion, is a measure of the stability of the anion. A positive electron affinity indicates that the anion is more stable than the neutral species.

[2] The large body of work on negative ions in the nearly four decades since Wildt's papers is reviewed in H. S. W. Massey's book, *"Negative Ions"* [8]—an excellent resource on atomic and molecular negative ions, including their modes of formation, occurrence, and applications.

form negative ions by the simple process of radiative electron attachment[3] at detectable abundances in dark molecular clouds [14, 15]. These studies were followed by ones which considered the chemical implications of the formation of large molecular anions in dense clouds, as well as the heating of diffuse molecular clouds by photodetachment of the negative ions [16, 17]. In 1998 five optical Diffuse Interstellar Bands (DIBs; [18]) were assigned to the pure carbon chain C_7^- based on gas-phase laboratory spectra [19]. Although this identification was later ruled out on astronomical grounds [20], it stimulated interest in negative molecular ions in space, and led to renewed theoretical, experimental, and observational work [21–26]. It is ironic that a few years prior to the C_7^- assignment, the first molecular anion had been detected in space, but more than a decade would pass before its eventual identification.

1.2 The B1377 problem and the identification of C_6H^-

Nearly half of the known interstellar and circumstellar molecules have been found in the thick dusty shell around the evolved carbon star IRC+10216, many of which, including the magnesium radical MgNC and the carbon chain radicals C_3N, C_4H, C_5H, C_6H[4], and C_8H[5] were first detected as unidentified radio lines [12, 13, 28, 30, 31]. In 1995 Kawaguchi et al. [29] published an exten-

[3]Reactions of the kind $A + e \longrightarrow A^- + h\nu$; see also, Appendix D.

[4]The C_6H radical was identified in the dark cloud TMC-1 by Suzuki et. al [27] and subsequently identified in IRC+10216 [28]

[5]This molecule was also detected as an unidentified series in Kawaguchi et. al's survey [29].

sive molecular line survey of IRC+10216 between $28 - 50$ GHz, done with the Nobeyama 45 m telescope. Of the 188 lines detected in the survey, 38 were unidentified—among these were seven which formed a harmonic sequence. The molecule responsible for this unidentified series was designated B1377, because a rotational constant of 1377 MHz was derived from the data.

Several features of B1377 were notable: (i) the derived rotational constant, 1377 MHz, was only 1% smaller than that of the C_6H radical ($B = 1391$ MHz; [32]); (ii) the lines were devoid of any structure or substructure, indicating that B1377 was likely a closed-shell molecule with a $^1\Sigma$ electronic ground state, but because molecular lines in IRC+10216 are broad, the possibility of unresolved structure buried within the lines could not be ruled out; and (iii) the lines were separated in frequency by ratios of integer quantum numbers—the signature of a linear closed-shell molecule—in favor of the second point, but still insufficient to rule out hyperfine structure present in some closed-shell molecules. So it was clear that high-resolution data were needed to advance the identification of B1377.

In 2006 July we observed in the cold dark molecular cloud TMC-1 with the NRAO 100 m Green Bank Telescope (GBT), two lines which coincided exactly in frequency with those derived from higher frequency lines of B1377. The observations toward TMC-1 were at high spectral resolution, because molecular lines in this source are narrow. With frequencies predicted from the astronomical data (i.e., seven lines in IRC+10216 and two in TMC-1) we conducted a search for B1377 with our laboratory spectrometers in discharges

through standard hydrocarbon precursors, acetylene and diacetylene (diluted in argon or neon). Under the right conditions (discussed in Chapter 3) the search yielded 17 lines of B1377 at precisely the frequencies derived from the astronomical series, but with higher accuracy, about 1 part in 10^7; two laboratory lines of B1377 are shown in Figure 1.1, along with the same lines observed in TMC-1. The B1377 series was attributed to the large carbon chain anion C_6H^-[6] based on the following observations: (i) a linear chain of six carbon atoms terminated by one H, neutral or ionized, is the only molecule consistent with the elemental composition of the hydrocarbon gases that produce B1377; lines of B1377 disappear when the precursor gas is deuterated, ruling out a pure carbon chain; (ii) the observed rotational constant corresponds to that of a chain with six and only six carbon atoms—one more or less yields a constant that is more than 40% too low or high; (iii) lines of C_6D^- were observed at precisely the deuterium shift (4.53%) predicted from the structure of C_6H^-, and the large deuterium shift is nearly identical to that found for the C_6H radical (4.55%; [34]), thus requiring a single H atom at one end of the chain; and (iv) no fine or hyperfine structure could be detected in the lower rotational lines in the laboratory at high spectral resolution, proving conclusively that B1377 was from a closed-shell molecule with a $^1\Sigma$ electronic ground state: neutral $C_6H(^2\Pi)$ and the C_6H^+ cation lack the required closed-shell symmetry—the radio spectrum of the former is well known, while the latter is predicted *ab initio* and observed by electronic spectroscopy [35, 36] to be $^3\Sigma$, which would

[6]This work is reported in McCarthy et al. (2006; [33]).

require B1377 to have a far more complicated spectrum than that observed in the laboratory or in space.

This experimental evidence established beyond any reasonable doubt that C_6H^- is the carrier of B1377 discovered more than a decade ago in the molecular envelope of IRC+10216. In addition, our identification confirmed an earlier suggestion by Aoki (2000; [37]), which was based on a quantum chemical calculation, that C_6H^- was a likely candidate for B1377.

The first molecular anion in space is an unusual and surprising molecule, larger than nearly all the neutral molecules that have been found and larger than all the cations. Aoki's suggestion was received with little enthusiasm for many years because IRC+10216 is deficient in molecular cations[7]: if electroneutrality were to prevail—so the argument ran—then negative ions should be equally rare, and hence unlikely to be observed there[8]. When it did receive attention, however, the astronomical searches undertaken were for anions which were too small for efficient electron attachment (CCH^- and C_2^-; [25,26]). But a lesson learned here, and one which had been discussed in the literature, was that size confers stability, and the cross section for electron radiative attachment increases with molecular size, favoring the formation of large negative ions [16, 17]. Theoretical calculations had also shown that because of the large density of states, electron attachment tends to become efficient for chains with

[7]As Fig. 8 in ref. [38] shows, HCO^+, one of the most readily observed molecular cations is only marginally detected in IRC+10216

[8]See, e.g., the introductory remarks in ref. [39]

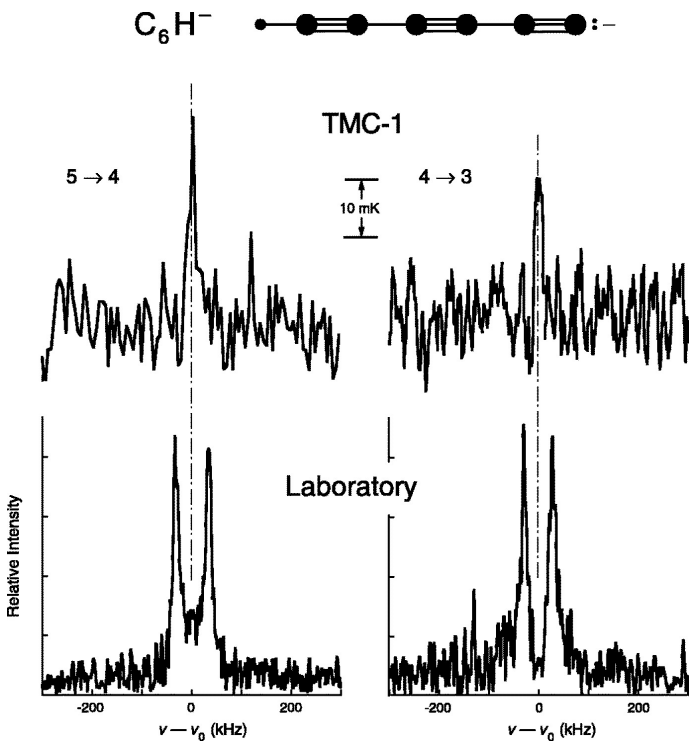

Figure 1.1: Two rotational transitions of C_6H^- (B1377) in TMC-1 and in the laboratory. Frequencies are relative to the laboratory rest frequencies, assuming the radial velocity of 5.8 km s^{-1} for TMC-1. The geometrical structure of C_6H^- showing the alternating triple and single bonds characteristic of acetylenic chains, with the two dots on the terminal carbon denoting the approximate location of the paired electrons, is displayed on top. The laboratory lines were obtained in 20 min of observation; the rest frequency of the transition is the average of the two components of the double-peaked line shape, a splitting that results from the Doppler shift of the fast-moving supersonic molecular beam relative to the two traveling modes composing the Fabry-Pérot cavity. The TMC-1 spectra were obtained by position-switching for 12 hr; the lines agree in frequency with those from the laboratory to about 4 kHz, approximately one-half of the 6 kHz channel-width used for the TMC-1 observations. Owing to the low line density in TMC-1, the probability that either line is due to a chance coincidence is $\leq 10^{-2}$, and the joint probability is $\leq 10^{-4}$, so a misidentification is highly improbable.

six carbon atoms or more [22]. Two spectroscopic factors, discussed in detail in Chapter 3, also favor detection of linear carbon chain anions: the simplification of the partition function upon electron attachment and the large gain in polarity over the neutral radical make lines of the anion several times stronger than those of the radical.

1.3 Recent work on linear closed-shell anions

Most interstellar molecules have been discovered by radio astronomy, with laboratory rotational spectroscopy providing conclusive support for their identification. Molecular anions remained unidentified until recently, largely because of the lack of high-resolution laboratory data required to guided radio astronomical searches. More than 1000 molecular anions have been studied at low resolution by photoelectron spectroscopy, which yields the electron affinity [40]. Fewer than 20, however, have been detected at high resolution from their optical or infrared spectra or both (cf. [41]), and only two simple diatomic anions—OH^- and SH^-—have been produced at sufficiently high densities to allow detection of their pure rotational spectra [42, 43].

The identification of C_6H^- suggested that structurally similar anions might be found in the radio band. The rotational spectra of five other anions, all carbon chains or related molecules, have now been measured to high accuracy in the laboratory, increasing fourfold the number of molecular anions detected by rotational spectroscopy. As Figure 1.2 shows, the carbon chain anions are of two kinds: four belong to the homologous acetylenic series $C_{2n}H^-$

starting at C_2H^-, and two, CN^- and C_3N^-, to the isoelectronic nitrile series $C_{2n+1}N^-$. All possess large electron binding energies (3 eV or higher), and have closed-shell ($^1\Sigma^+$) electronic ground states, with the extra electron occupying a tightly bound σ-orbital of very high s character on the terminal carbon atom, constituting a highly stable arrangement of valence electrons [24]. And all, with the exception of CN^-, have large dipole moments yielding strong lines in the radio band.

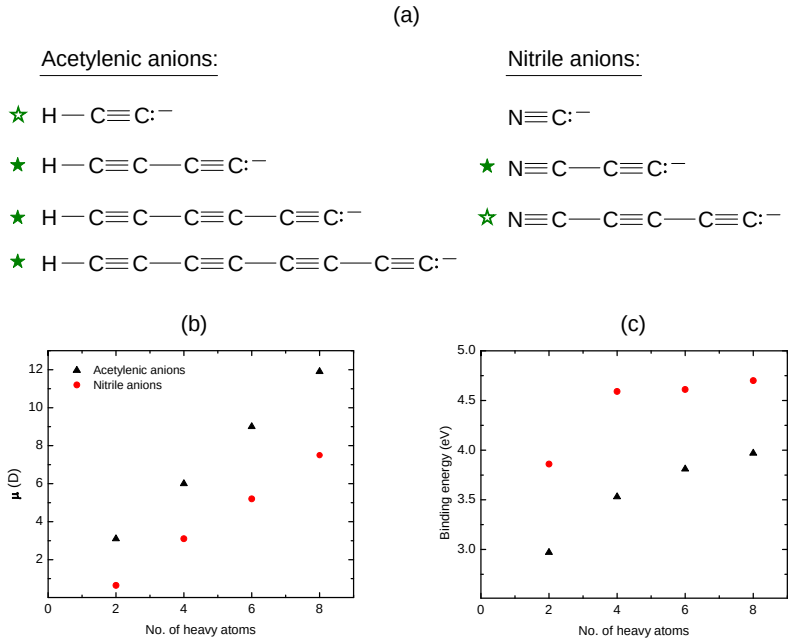

Figure 1.2: Carbon chain anions detected in the radio band; all but C_5N^- have been detected in the laboratory. (a) Molecular geometries of carbon chain anions, showing the characteristic triple and single carbon-carbon bonds of acetylenic chains; filled stars indicate confirmed astronomical identification, and empty ones indicate a tentative one; (b) dipole moments (μ); and (c) binding energies of the anions. The C_7N^- ion is included in (b) and (c) to show the trends in the properties.

The availability of accurate laboratory rest frequencies has allowed deep radio astronomical searches for these anions, and besides C_6H^-, three more—C_4H^-, C_8H^-, and C_3N^-—have now been conclusively identified in space. Tentative evidence is also claimed for two others: C_2H^- and C_5N^- (which has so far eluded detection in the laboratory). The larger anions C_6H^- and C_8H^- are surprisingly abundant, from a few percent to a few tens of percent, relative to their parent neutral radicals. The fractional abundances of the smaller ones C_2H^- and C_4H^- relative to the neutral species, however, are only a few thousandths to a few hundredths of a percent. As the processes of formation and destruction of negative ions in space are not well understood, the explanations for this conspicuous split are as yet only plausible ones, and the same theory [22] that works fairly well for larger anions, fails to reproduce the sharp drop observed in the anion-to-neutral ratio of smaller chains.

The detection of new anions in space has been closely followed by the discovery of new sites of anions. A galactic survey of the most readily observed molecular anion, C_6H^-, has been started, and has added two dark molecular clouds to the list of known sources of anions, raising the number of such sources nearly twofold [44]. The results also suggest that anions may be detected in many other sources; they are likely to be found with deeper observations, or with more comprehensive surveys, or both. In addition, the survey has resulted in a significant increase in the number of sources of the related carbon chain radicals C_4H and C_6H, which were previously known only in a few sources.

The spectroscopic characterization of the carbon chain anions in the

laboratory was guided by high-level coupled-cluster quantum chemical calculations, which predict the ground state rotational constants of these closed-shell molecules remarkably accurately—within 0.1% of those observed—an order of magnitude better than the 1% accuracy typical less than 20 years ago. The net result, not surprisingly, has been a nearly tenfold reduction in search time for the anions. The calculations also yield fairly precise estimates of the centrifugal distortion constants, allowing prediction of successive rotational transitions to within a line width for searches in the millimeter-wave band. In addition, the calculations yield precise estimates of electrical properties: dipole moments for all, and quadrupole coupling constants for those with nitrogen and deuterium.

The work here is an example of the powerful interaction between theory, experiments, and astronomical observations, which has advanced the identification of molecules in space. This interplay is likely to assume greater importance as new astronomical molecules unknown to the terrestrial spectroscopist are found and require conclusive identification. The number of such molecules is expected to increase with new sensitive telescopes such as the Herschel Space Observatory and the Atacama Large Millimeter Array. The three fields working together would go far in solving new puzzles which the next generation of instruments will find in the rich chemical inventory of the interstellar gas, in particular the exotic molecules not readily observed in the terrestrial laboratory.

Chapter 2

Coupled-Cluster Calculations of Carbon Chain Anions

2.1 Introduction

Calculations employing higher-order approximations of coupled-cluster theory[1] to treat electron correlation have been found to yield accurate and reliable predictions of the spectroscopic properties of small to medium-sized molecules. One of the most widely used coupled-cluster methods is the coupled-cluster singles and doubles model augmented by a perturbative treatment of triple excitations CCSD(T) [46] which, in combination with the use of large basis sets, has become the standard for accurate calculations[2]. Rotational constants calculated using the "CCSD(T)/large-basis-set" approach have typically been well within one percent of the experiment, and even more accurate results were obtained for closed-shell molecules [47–50]. Owing to the accuracy of its results, this approach has been quite useful—and sometimes crucial—in the identification of new molecules in the laboratory [51–54]. Even a radio

[1]The reader is referred to ref. [45] for a review of coupled-cluster theory.

[2]Because it gives results of comparable accuracy to higher order coupled-cluster methods at a nearly tenfold lower computational cost, the CCSD(T) method is considered a good compromise. However, even this method becomes cumbersome for molecules with more than about 20 carbon atoms.

astronomical search for the small molecular anion CCH^- has been based on frequencies predicted from CCSD(T) rotational constants [26]. Most recently, a CCSD(T) calculation was used to buttress the assignment of an unidentified series of lines observed in IRC+10216 to the C_5N^- anion, for which laboratory data are not yet available [55].

The large carbon chain anion C_6H^- was also first suggested as a plausible carrier of B1377 on the basis of a quantum chemical calculation [37]. Although the theoretical rotational constant was very close to that of B1377, the calculation involved empirical scaling of the equilibrium rotational constant, and did not provide the vibrational corrections to better estimate the observed rotational constant. Following the detection of two transitions of B1377 in TMC-1 and many more in the laboratory, an independent high-level CCSD(T)/large-basis-set calculation of C_6H^- yielded a ground state rotational constant within 0.1% of B1377.

The CCSD(T)/large-basis-set approach worked well for other linear closed-shell anions as well. Indeed, the calculations predicted the spectroscopic constants of the anions now known to remarkable accuracy. Specifically, the calculated ground state rotational constants, B_0, were within 0.1%, and centrifugal distortion constants, D_J, generally within 10% of those observed. As B_0 and D_J determine the frequencies of rotational lines, the availability of accurate calculations has speeded up considerably the laboratory detection and identification of the new anions. Besides these two crucial spectroscopic parameters, the permanent electric dipole moments (μ) and quadrupole coupling

constants (eQq) were also calculated. The dipole moment determines the intensity of rotational lines, from which molecular abundances can be estimated. In molecules with quadrupolar nuclei, the eQq provides a characteristic spectral signature; the calculated eQq for the ^{14}N-bearing anions, CN^- and C_3N^-, were found to be within a few percent of those derived from measurements.

Here I present the essentials of these calculations, and discuss the results which have aided the spectroscopic characterization of the anions. The papers on the laboratory detection of the carbon chain anions included only brief notes on the calculations. Since the publication of those reports, more extensive calculations than those here have been done by Botschwina and coworkers (cf. [56]), using the CCSD(T)/large basis set approach. I shall refer to their calculations, and discuss them wherever a comparison is warranted.

2.2 Methodology

The calculations were carried out using the CCSD(T) method in conjunction with large correlation-consistent basis sets developed by Dunning and coworkers [57–61]. Used with the CCSD(T) method, these have been shown to yield fairly precise estimates of the structure and properties of molecules. The basis sets are of two kinds[3]: (i) cc-pVXZ, where X=D,T, and 4, and

[3]The 'cc-p' is short for 'correlation-consistent polarized', and the 'V' indicates their "valence only" nature—i.e., they are optimized only with respect to the valence correlation energy of the atom. When the cc-pVXZ basis sets are augmented with functions for including the correlation energy from inner shell atomic electrons, they are designated cc-pCVXZ, where the 'CV' stands for 'core-valence'.

(ii) cc-pCVXZ, with X=D,T,4 and 5. The largest basis sets used were cc-pCVQZ for CCH^-, aug-cc-PCV5Z for CN^-, cc-pVQZ for C_3N^-, and cc-pVTZ for C_4H^-, C_6H^-, and C_8H^-, and results from these basis sets are reported in the tables. All electrons were correlated in the calculations irrespective of the type of basis set used. The ACES II package of *ab initio* quantum chemical programs developed by Stanton, Gauss, and coworkers [62, 63] was employed for all calculations described below.

2.2.1 Equilibrium structures, cubic force fields, and vibrational corrections

A quantum chemical calculation yields the optimized equilibrium structure of a molecule, allowing determination of the equilibrium rotational constant, B_e is given by

$$B_e = \frac{h}{8\pi^2 I_e} \ , \tag{2.1}$$

where I_e is the moment of inertia of the molecule about its center-of-mass. The rotational constant derived from the spectra however, is affected by molecular vibration. A correction for vibrational effects is therefore required for the accurate prediction of rotational line frequencies for laboratory searches. The centrifugal distortion of the rotating molecule must also be accounted for, as it often results in a shift in line frequencies of several MHz—i.e., several line widths in the millimeter-wave band.

Ground state rotational constants B_0 and the centrifugal distortion

constant D were calculated as follows[4]. The equilibrium structures, corresponding to a minimum on the molecular potential energy surface (within the Born-Oppenheimer approximation), were obtained by minimizing the total molecular energy as a function of the nuclear coordinates. The molecule was considered to be at the equilibrium geometry when all forces on the atoms were below about 10^{-5} atomic units. The harmonic force field was calculated, and the normal coordinates determined. Cubic force constants were evaluated by numerical differentiation of analytic second derivatives calculated at points displaced along the normal coordinates; the quadratic force field yielded the centrifugal distortion constant (D_J). The vibration-rotation interaction constants (α_r) were then determined from second-order vibrational perturbation theory (VPT2; [65]). Finally, B_0[5]—the rotational constant in the ground vibrational state ($\upsilon = 0$)—was estimated using the familiar VPT2 expansion in powers of the vibrational quantum number υ:

$$B_\upsilon \;=\; B_\mathrm{e} - \sum_{r=1}^{3r-5} \alpha_r \left(\upsilon_r + \frac{d_r}{2} \right) + \ldots \tag{2.2}$$

where the sum is over the normal modes of vibration r, and d_r is the degeneracy of the r-th mode[6]. Here it should be noted that the individual α_r obtained by this method are not neccesarily reliable owing to contributions from Coriolis resonances. These resonances cancel out [66] in the sum in eq 2.2, so the

[4]Further details can be found in ref. [64]

[5]Except in this chapter, the subscript 0 will be dropped from the ground state rotational constant, which will be simply denoted B. Similarly, D_J will be denoted D.

[6]$d_r = 1$ for stretching vibrations and 2 for bending vibrations.

total vibrational correction may be calculated reliably [67]. This correction, hereafter denoted ΔB_0, was then subtracted from B_e to obtain B_0.

2.2.2 Molecular properties: dipole moments and quadrupole coupling constants.

Besides B_e, B_0, and α_r, two electric properties were calculated. These are: i. the equilibrium electric dipole moments μ_e of all anions, and ii. the electric quadrupole coupling constants $eQq(^{14}\mathrm{N})$ for CN^- and C_3N^-, and $eQq(\mathrm{D})$ for C_4D^-.

The equilibrium dipole moment, in the molecular center-of-mass frame, is given by

$$\mu_e = \sqrt{\mu_x^2 + \mu_y^2 + \mu_z^2}. \tag{2.3}$$

The components μ_x, μ_y, and μ_z are the first derivatives of the total molecular energy, with respect to the electric field strength ϵ along an axis i:

$$\mu_i = -\frac{\partial E}{\partial \epsilon_i} \ . \tag{2.4}$$

In a linear molecule, the molecular axis is chosen to coincide with the z-axis, so that $i = z$ in the above equation.

The electric quadrupole coupling χ_{ij} from a nucleus n is given by

$$\chi_{ij}(n) = -\frac{eQ_n q_{ij}^n}{\hbar}, \tag{2.5}$$

where e is the electron charge, Q_n is the quadrupole moment of the nucleus n, and q_{ij}^n is the gradient of the electric field along the molecular axis. From

the calculated zz-component of the electric field gradient q^n_{zz} (in atomic units), and Q_n (in barn[7]) from standard tabulations [68], the eQq (in MHz) is given by

$$eQq(n) = 234.964730 \times Q_n q^n_{zz} \tag{2.6}$$

The calculated $eQq(^{14}\mathrm{N})$ and $eQq(\mathrm{D})$ are given in Table 2.6.

2.3 Results and Discussion

2.3.1 Equilibrium structures, B_0, and D_J

Table 2.1 lists the equilibrium bond lengths of all six anions discussed here, as well as the structures calculated recently by Botschwina et al., shown in parentheses (see Table 2.1 for references). The anions C_4H^- and larger show the triple-single-triple bond alteration characteristic of acetylenic chains. The C–C triple bonds are longest near the terminal carbon atom and shorten somewhat at the carbon nearest the hydrogen atom, whereas the C–C single bonds display the opposite trend.

Consider first the acetylenic anions. The carbon-carbon bond lengths from both sets of calculations generally agree to within 0.002%; the largest differences are seen between the CC2 ($0.006 - 0.008\%$) and CC4 (0.005%) bond lengths. The differences between the CH bond lengths for all but the smallest anion, C_2H^-, are about 0.007%. The agreement is somewhat better for the nitrile anions: the CC bond lengths agree to within 0.002%. The CN

[7] 1 barn = $10^{24}\mathrm{cm}^2$.

bond in C_3N^- also agrees to within 0.001%; that in CN^-, however, differs by nearly 0.004%.

Table 2.1: CCSD(T) equilibrium structures of acetylenic and nitrile anions[a].

	Molecule					
Bond[b]	C_2H^- [c]	C_4H^- [d]	C_6H^- [d]	C_8H^- [d]	CN^- [e]	C_3N^- [e]
CC1	1.2460	1.2546	1.2592	1.2614		1.3663
	(1.2464)	(1.2568)	(1.2609)	(1.2634)		(1.3678)
CC2		1.3647	1.3489	1.3413		1.2516
		(1.3728)	(1.3566)	(1.3488)		(1.2513)
CC3		1.2231	1.2328	1.2373		
		(1.2251)	(1.2343)	(1.2390)		
CC4			1.3571	1.3435		
			(1.3629)	(1.3483)		
CC5			1.2197	1.2300		
			(1.2219)	(1.2314)		
CC6				1.3583		
				(1.3640)		
CC7				1.2174		
				(1.2196)		
CH	1.0692	1.0543	1.0551	1.0557		
	(1.0697)	(1.0618)	(1.0614)	(1.0618)		
CN					1.1775	1.1716
					(1.1814)	(1.1708)

[a]Basis sets: the cc-pCVQZ basis set was used for C_2H^-, and cc-pVTZ for the larger anions; the aug-cc-pCV5Z basis set was used for CN^-, and the aug-cc-pVQZ for C_3N^-.
[b]Bond lengths are in Å; bonds are numbered starting at the terminal C atom for the acetylenic anions, and at the N atom for the nitrile anions.
[c]Values in parentheses are CCSD(T)/cc-pCVQZ value from ref. [69]
[d] CCSD(T)/aug-cc-pVQZ values from refs. [70]
[e]CCSD(T)/cc-pVQZ values from ref. [71].

Two factors contribute to the differences between the equilibrium structures of the carbon chain anions (Table 2.1) C_4H^- and larger from the two data sets. First, a smaller basis set, cc-PVTZ, was used in our calculations than that used by Botschwina et. al (cc-pVQZ). Second, all electrons were cor-

related in our calculations, even when the "valence only" cc-pVTZ basis set was used; it is customary to neglect the core electrons [8], i.e., the lowest-energy molecular orbitals, when using cc-pVXZ basis sets[9]. Despite the slightly different approach, however, the present calculations yield B_e that are close to those calculated by Botschwina et al. [56]. In fact, correlating all electrons with the use of the cc-pVXZ basis sets tends to yield more accurate structures—since core-correlation is treated, albeit partially. This could be proven by performing the all-electron calculations with the larger basis cc-pVQZ sets. For larger molecules, such calculations rapidly become time consuming, but can nonetheless be done for anions here through C_6H^-. The equilibrium geometries reported here are reliable and have yielded precise estimates of the rotational constants—even those of the isotopically substituted anions (Table 2.3) —making conclusive laboratory assignments possible.

Table 2.2 summarizes the B_e, B_0, and total vibrational corrections (ΔB_0) along with the ground-state rotational constants derived from the laboratory data; the individual α_r and harmonic frequencies are collected in Appendix A. Although ΔB_0 is only a fraction of B_e, its contribution becomes important when predicting rotational lines at high frequencies. In all cases, the calculated B_0 agree with the experimental ones to better than 0.1%. Sim-

[8]The inner shell electrons of the atoms: for atoms Li to Ne, this is typically the $1s$ atomic orbital

[9]The usual justification for this is that the core electrons are less sensitive to their environment than are the valence electrons. Hence the error resulting from neglecting the contribution of the former is nearly constant across molecules composed of the same elements.

ilarly, Table 2.3 gives the B_e, B_0, and ΔB_0 for the three larger deuterated acetylenic anions, and the agreement is comparable to that for the normal species.

Table 2.2: CCSD(T) rotational constants and vibrational corrections for the anions (MHz).

Molecule	B_e [a]	B_0^{calc}	ΔB_0^{calc} [b]	B_0^{exp} [d]	$\Delta^{exp-calc}(\%)$
C_2H^-	41,820	41,636	584	41,639.237(4)	0.01
C_4H^-	4,658	4,654	4	4,654.9449(2)	0.02
C_6H^-	1,376	1,377	−1	1,376.86298(7)	0.01
C_8H^-	582.6	583.2	−0.6	583.34014(8)	0.06
CN^-	56,401	56,152	249	56,132.7504(35)	0.03
C_3N^-	4,853	4,848	4.6	4,851.62183(20)	0.07

Note: all constants are in MHz.
[a] From equilibrium structures in Table 2.1
[b] Basis sets used in the cubic force field calculations: cc-pCVQZ (CCH^- and CN^-); cc-pVTZ (C_3N^-); cc-pVDZ (C_4H^- and C_6H^-)
[c] From an SCF/DZP force field calculation.
[d] See refs. in Table 3.3.

Table 2.4 summarizes the centrifugal distortion constants of the anions. As can be seen, the calculated D are within $5-20\%$ of those derived from the experimental data. Larger discrepancies are seen for the two largest anions. In C_8H^- this may be attributed to the lower level of theory (SCF/DZP) employed in the calculation of the force field. That for C_6H^- is also probably due to the smaller basis set (cc-pVDZ) used. The use of a much larger basis set (cc-pVQZ; ref. [70], however, only improves the estimate of D_J by less than 10%. A more systematic study of the effects of the level of theory used might help to properly quantify and explain the deviation of the small centrifugal distortion

terms.

Table 2.3: CCSD(T) rotational constants for deuterated acetylenic anions (MHz).

Molecule	B_e [a]	B_0^{calc} [c]	ΔB_0^{calc} [b]	B_0^{exp} [d]	$\Delta^{exp-calc}(\%)$
C_4D^-	4,327	4,322	5	4,324.02014(2)	0.05
C_6D^-	1,313	1,314.4	−1	1,314.47424(7)	0.005
C_8D^-	563	563.9	−0.9	563.90854(8)	0.002

Note: all constants are in MHz.
[a] From equilibrium structures in Table 2.1
[b] Basis sets used in the cubic force field calculations: cc-pCVQZ (CCH^- and CN^-); cc-pVTZ (C_3N^-); cc-pVDZ (C_4H^- and C_6H^-)
[c] Scaled using B_0/B_e from the normal species in Table 2.2. [d] See refs. in Table 3.3.

Table 2.4: Calculated and derived centrifugal distortion constants, D_J.

Molecule	$10^6 D_J^{calc}$	$10^6 D_J^{exp}$ [a]	$\Delta^{exp-calc}(\%)$
C_2H^-	93,000	96,970(90)	4.1
C_4H^-	550	587.5(1)	6.5
C_6H^-	27	32.35(1)	18.4
C_8H^-	3.5	4.3(2)	18.6
CN^-	185,230	185,790(15)	0.4
C_3N^-	627	685.92(10)	8.6

Note: constants are in MHz.
[a] See Table 3.3 for references.

2.3.2 Electric dipole moments (μ_e) and quadrupole coupling constants (eQq)

The equilibrium electric dipole moments of the acetylenic anions, along with those calculated by Botschwina et al., are given in Table 2.5. In all cases, the two sets of values agree to better than 5%. As the dipole moments have

not been measured, no comparison with experiment is available at this time.

Table 2.5: CCSD(T) equilibrium electric dipole moments of acetylenic anions[a].

Molecule	μ_e (D)	
	This work	Previous & recent work [b]
C_2H^-	3.1	3.1
C_4H^-	6.0	6.3
C_6H^-	9.0	9.0
C_8H^-	11.9	12.4
CN^-	0.65	0.65
C_3N^-	3.1	3.1

[a]Dipole moments are calculated at the equilibrium geometries reported in Table 2.1.
[b]References: C_2H^- [69]; C_4H^-–C_8H^- [70]; CN^- [72]; C_3N^- [71].

Table 2.6 lists the calculated equilibrium quadrupole coupling constants of ^{14}N in CN^-, C_3N^-, and that of D in C_4D^-. Excellent agreement, to better than 2%, is found for CN^- and C_3N^-. That for C_4D^-, of about 3%, is somewhat worse. These discrepancies are probably due to vibrational effects—the experimental values are measured in the ground vibrational states, whereas the values calculated here are at the equilibrium geometries. The poorer agreement for eQq(D) compared with eQq(N) may arise because the effect of zero-point vibrations are larger for D compared with those for N. More accurate estimates could be obtained by including zero-point vibrational corrections using VPT2 [65]. Similar calculations carried out for HC_3N and DC_3N also yield eQq's in precise agreement with experiment [73].

Table 2.6: Electric quadrupole coupling constants for CN^-, C_3N^-, and C_4D^-[a], and prediction for CCD^-.

		eQq (MHz)	
Molecule	q^a(au)	Calculated	Measured
CN^-	−0.8887	−4.25	−4.238(32)
C_3N^-	−0.6947	−3.30	−3.248(5)
C_4D^-	0.3373	0.21	0.204(6)
CCD^-	0.3453	0.22	

[a]The electric field gradient, calculated at the geometries reported in Table 2.2.

2.4 Conclusions

Accurate estimates of B_0 was obtained when the vibrational corrections calculated from second-order perturbation theory were applied to B_e. The calculated B_0 was typically within 0.1% of that determined by experiment. The centrifugal distortion constants, D_J, from the quadratic force fields were also predicted fairly well—to better than 20%. Together, the theoretical B_0 and D_J yield rotational frequencies of successive transitions to within a few pressure-broadened line widths (i.e., within a few MHz at 300 GHz). The upshot is that laboratory searches of many anions are now nearly ten times faster than those possible only 20 years ago.

The equilibrium dipole moments of the carbon chain anions are found to increase nearly linearly with chain length, and are expected to become very large for longer members of the homologous series. Recent calculations predict a dipole moment of nearly 20 D for $C_{12}H^-$ [56], and nearly 17 D for $C_{13}N^-$ [71]. The dipole moments reported here and from similar calculations

[56, 70, 71] are in very good agreement with each other, and—in the absence of experimental values—are crucial to the calculation of molecular line intensities and abundances in the radio band.

Additionally, $eQq(^{14}\mathrm{N})$ in CN^- and C_3N^-, as well as $eQq(\mathrm{D})$ in C_4D^-, were predicted fairly precisely, aiding the assignment of the quadrupole hyperfine structure in the lowest rotational transitions of these molecules. The calculations of CN^- are in excellent agreement with earlier ones on this species [74], and to the best of my knowledge, the calculations here are the first ones reported for the two larger species. Here we also predict an $eQq(\mathrm{D})$ for C_2D^-, with an expected accuracy of a few percent. Few theoretical papers report properties useful to the assignment of rotational spectra. Since the electric field gradient at atomic centers can be readily calculated, eQq from quadrupolar nuclei can be easily obtained as well and should be included in papers directed at rotational spectroscopy.

The anions studied here are simple, closed-shell systems, amenable to sophisticated theoretical characterization. Now that high-resolution laboratory data are available for these molecules, the calculations can be systematically calibrated and put on a more quantitative, and ideally, statistical basis. Such efforts are already underway for linear carbon chain anions [56, 70, 71]. A more critical evaluation of the accuracy of CCSD(T) calculations of anions might become possible with the detection of the rotational spectra of new molecular anions. Similar calculations can be done more generally for anions, including nonlinear and planar ones, with an accuracy comparable to that

for linear anions. Possible candidates which may be of interest to laboratory astrophysicists are CH_3CC^-, c-C_3H^-, and CH_2CN^-; existing calculations on these and other closed-shell anions can probably be improved upon and better predictions of rotational spectra made available.

The highly accurate calculations of the spectroscopic constants of carbon chain anions reported here illustrate the power and efficacy of high-level coupled-cluster calculations in guiding laboratory searches of molecules. Indeed, the rotational spectroscopy of these molecular anions has benefited substantially from these calculations: the identification of C_6H^-, as well as the rapid detection of five other related anions [75–78] has been possible largely because of the availability of accurate theoretical predictions.

Chapter 3

Rotational Spectroscopy of C_4H^-, C_6H^-, C_8H^-, and C_3N^-

3.1 Introduction

The rotational spectra of six new carbon chain anions shown in Figure 1.2 have been detected within the past three years. Four are the first negatively charged molecules to be identified in space, starting with C_6H^-—which motivated studies of the other structurally related molecular anions; accounts of these detections have appeared in a series of papers since 2006. In this chapter I discuss the laboratory work on these four anions [1], including data on isotopically substituted species and measured rotational line frequencies that for brevity were excluded from the original papers. The papers emphasized the identification of these anions beyond any reasonable doubt, and through a series of assays and tests, demonstrated that the assigned lines could not be from any other molecule. These assays and their role in clinching the identification of these molecules on the basis of the spectroscopic evidence are also discussed here.

[1] The original papers on CCH^-, CN^-, and the hyperfine sructure of C_3N^- and C_4D^-, are cited in the text.

The two well-known techniques of long path absorption spectroscopy of DC glow discharges in the millimeter-wave band and Fourier transform microwave (FTM) spectroscopy of a supersonic molecular beam in the centimeter-wave band were used to observe rotational lines of carbon chain anions. I begin with a brief description of these experiments and the conditions required to produce the anions. Table 3.1 lists anions detected in the two experiments, and provides references to the laboratory work.

Table 3.1: Laboratory detections of carbon chain anions in the radio band.

Molecule	Rare Isotope	No. of Lines[a]	Frequency Bands (GHz) FTM	Frequency Bands (GHz) Free Space[b]	References
Acetylenic anions:					
C_2H^-.....	^{13}C	5(6)	···	$83-417$	[79]
C_4H^-.....	D	19(16)	$8-38$	$83-363$	[75]
C_6H^-.....	D	17(5)	$8-23$	$145-188$	[33]
C_8H^-.....	D	9(9)	$9-19$	···	[75]
Nitrile anions:					
CN^-.....	···	5	···	$112-450$	[77]
C_3N^-.....	···	16	$9-30$	$97-378$	[78]

[a]Lines of isotopically subsituted species are in parentheses. [b]Millimeter-wave spectrometer.

3.2 Experimental Methods

3.2.1 Millimeter-wave Absorption Spectroscopy

3.2.1.1 Detection of carbon chain anions by double-pass measurements

Figure 3.1 shows a schematic of the free space millimeter-wave spectrometer (cf. [80]) used to observe rotational transitions of the carbon chain anions. Solid state Gunn diode oscillators producing millimeter-wave radiation in the range $70-145$ GHz phase locked to a high harmonic of a frequency

synthesizer (HP 8662A) are tuned over a maximum range of 220 MHz, efficient multipliers then generating the power necessary to observe transitions up to 500 GHz. The resulting radiation makes two passes through the absorption cell: the source beam passes through a plane wire polarizer, is focused into the cell by a teflon lens, and is incident on a dihedral mirror; the return beam, with its plane of polarization rotated by 90°, reflects off the polarizer and is focused on a liquid-He-cooled InSb hot-electron bolometer [81]. A computer sweeps the synthesizer (HP 8662A) through the desired frequency range and displays the baseline-subtracted spectrum. Frequency modulation (at $f = 49$ or 95 kHz) of the Gunn and phase-sensitive detection at the second harmonic of the modulation frequency reduce $1/f$ noise and large amplitude standing waves between the source and detector, yielding a line shape that is approximately the second derivative of a Lorentzian.

3.2.1.2 Determination of the molecular charge by single-pass measurements

We were able to directly determine the charge of three anions, CN^-, C_4H^-, and C_3N^-, by detecting them in an arrangement in which the the dihedral mirror is removed and millimeter-waves are detected in a single pass through the cell. The axial electric field, typically $5 - 15$ V cm^{-1} [82], in the positive column of the glow discharge, accelerates the ions and results in a Doppler shift in the line frequencies of

$$\delta\nu = \nu_0 \frac{v_a}{c} \tag{3.1}$$

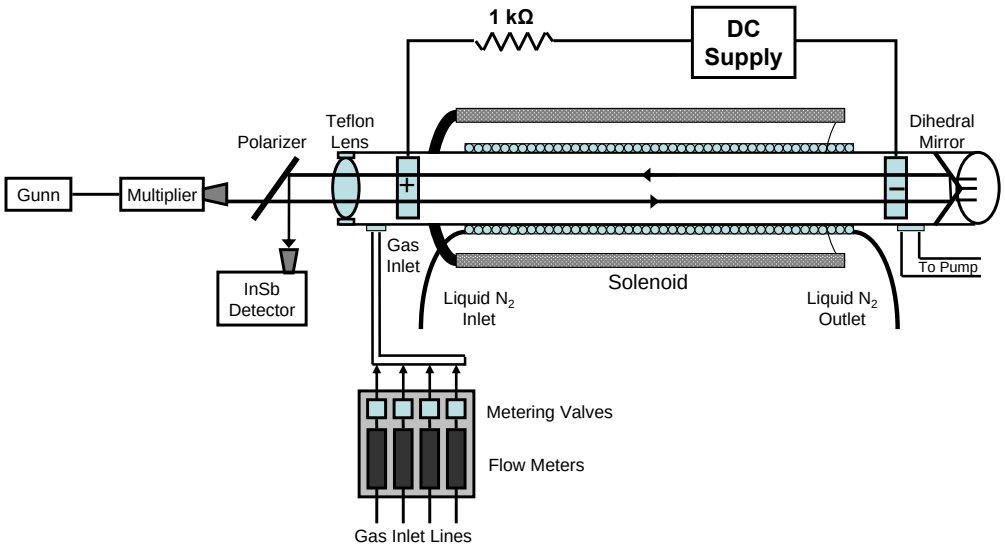

Figure 3.1: Simplified schematic of the free space millimeter-wave spectrometer showing the discharge cell, the radiation source, and the detector; the optical path of the millimeter-wave radiation is also shown. Finer details of the apparatus can be found in refs. [80] and [81].

where v_a is the axial drift velocity of the ion, ν_0 is the line center frequency, and c is the speed of light.

3.2.1.3 Anion production in the glow discharge

The anions are produced in a low current DC glow discharge through a flowing mixture of the organic precursor and a buffer gas (Table 3.2) between hollow cylindrical stainless-steel electrodes driven by a current-controlled high-voltage power supply (Glassman series KL/Spellman SR 6). Lines of the anions are detected at discharge currents that are $3-5$ times lower than those which produce the strongest lines of the neutral radicals. The temperature of the 3

m long, 15 cm diameter glass discharge cell is maintained at a desired value between 100 and 300 K by circulating liquid nitrogen through a copper jacket around the cell, yielding total pressures in the range $5-20$ mTorr. Under these conditions, the lines of the anions are several times weaker than those of the corresponding neutral radicals, but are still observed with high signal-to-noise ratios after modest integration.

Table 3.2: Production of anions in the free space spectrometer.

Anion	Precursor/ Buffer gas	Discharge Current (mA)	Cell Temp. (K)	Anion/Neutral Ratio	Number density ($10^5 cm^{-3}$)
C_2H^-	HCCH/Ar	150	120	0.1	1,000
C_4H^-	HCCH/Ar	150	100	0.14	500
C_6H^-	HCCH/Ar	150	150	0.5	7
CN^-	NCCN/Ar	25	200	1.0	20,000
C_3N^-	$HC_3N/Ar/N_2$	20	250	2.0	300

3.2.2 Fourier Transform Microwave Spectroscopy

Centimeter-wave rotational lines of the four larger carbon chain anions were detected in emission by Fourier transform microwave (FTM) spectroscopy of a supersonic molecular beam (Table 3.3). Figure 3.3 shows a simplified diagram of the liquid-nitrogen cooled FTM spectrometer and the pulsed discharge nozzle that are described in detail elsewhere [83]. A dilute organic vapor in a buffer gas held at a high backing pressure behind the pulsed solenoid valve (General Valve) of the discharge nozzle is allowed to expand into the high vacuum of the cavity of the spectrometer. The molecules in the resulting supersonic beam are irradiated with a short microwave pulse ($1\mu s$) synchronized

with the passage of the gas pulse through the cavity. The microwave pulse has sufficient power to saturate allowed molecular transitions lying within the 1 MHz bandwidth of the high-Q confocal Fabry-Perot cavity. The free induction decay (FID) resulting from the relaxation of these molecules is then Fourier transformed to obtain a power spectrum and emission line profile. The Doppler shift of the molecular beam relative to the two traveling waves composing the confocal mode of the Fabry-Pérot cavity results in a double-peaked line shape for a given transition. The cavity mirrors and first-stage amplifier are cooled to 77K to reduce thermal noise and to increase the sensitivity to detect the generally weak lines of the anions.

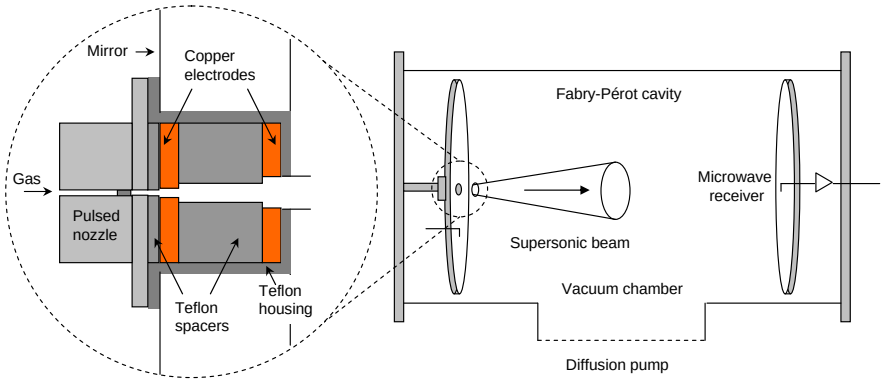

Figure 3.2: Simplified diagram of the liquid-nitrogen cooled Fourier transform microwave (FTM) spectrometer showing the confocal Fabry-Pérot cavity and the pulsed discharge nozzle. Adapted from ref. [83].

The anions were made in the throat of the supersonic nozzle by applying a low-current DC discharge to the short gas pulse. The production of the

anions is sensitive to the voltage and polarity of the discharge: the best anion signals were generally observed at a significantly lower voltage ($500 - 700$ V) than that which yields the strongest lines of the neutral parent radicals (1000 V)—an important finding; the polarity of the discharge was reversed relative to that for producing the radicals. The electrode close to the valve is maintained at a negative high voltage, and that further down in the expansion channel is grounded. The nozzle configuration and discharge conditions are nearly identical to those used to observe the photoelectron spectra of carbon chain anions in a similar discharge [84]. The total flow rate was about $20 - 25$ $cm^{-3}min^{-1}$ at standard temperature and pressure, the stagnation pressure behind the valve was 2.5 kTorr, and the nozzle was pulsed at a repitition rate of 6 Hz. Under these conditions, lines of the anions were detected with modest to fairly high signal-to-noise ratios after integration of a few minutes for C_4H^- to 90 minutes for C_8H^-.

Table 3.3: Production of anions in the FTM spectrometer.

Anion	Precursor/ Buffer gas	Discharge Current/Voltage (mA/V)	A/N Ratio	Number density (10^8/pulse)
C_4H^-	HC_4H/H_2	$10 - 20/600 - 700$	$0.12 - 0.3$	$10 - 30$
C_6H^-	HC_4H/Ne	$20/600$	1.0	1
C_8H^-	HC_4H/Ne	$10 - 20/600 - 700$	2.0	1
C_3N^- [a]	$HC_4H/HC_3N/H_2$	$10 - 20/500 - 700$	2.0	$\cdots$

From ref. [85].

3.3 Results

The linear geometries and closed-shell electronic ground states of the carbon chain anions result in simple rotational spectra marked by transitions that are separated by nearly harmonic intervals. The spectroscopic constants of the anions (Table 3.4) were derived from a linear least-squares fit to the observed lines (Table 3.5–3.8) using the standard expression [86]

$$\nu_{J+1\rightarrow J} = 2B(J+1) - 4D(J+1)^3, \tag{3.2}$$

where J is angular momentum quantum number of the lower level of the transition, B is the rotational constant, and D is the leading centrifugal distortion constant. From B and D alone the rotational transition frequencies of all of the anions here can be calculated to high accuracy over most of the radio band. A third term containing the sixth-order distortion constant, H, may be included in (3.2), but only at frequencies above 2 THz does it become significant for the two lightest anions, CCH^- and CN^- [77, 79].

3.3.1 C_4H^-

In the free space spectrometer, C_4H^- was produced in a DC glow discharge through HCCH and argon at a total pressure of $\leq$ 10 mTorr with the cell walls cooled to 100K, and an optimum dicharge current (150 mA) nearly three times lower than that which produces the strongest lines of C_4H (400 mA). Lines of C_4H^- were about 8 times weaker than either fine structure component of C_4H; the hyperfine structure of C_4H collapses at high J and is

Table 3.4: Spectroscopic Constants of Carbon Chain Anions (in MHz)

Molecule	B	$D \times 10^6$	eQq
Normal species:			
C_4H^-	4,654.9449(2)	587.5(1)	
C_6H^-	1,376.86298(7)	32.35(1)	
C_8H^-	583.34014(8)	4.3(2)	
C_3N^-	4,851.62183(20)	685.92(10)	-3.25^a
Isotopic species:			
C_4D^-	4,324.02014(2)	489.49(9)	$0.204(6)^a$
C_6D^-	1,314.47424(7)	36.04(223)	
C_8D^-	563.90854(8)	3.9(2)	

Note: Here and in the other tables, the 1σ uncertainties (in parentheses) are in units of the last significant digit. ^{a}From ref. [85]

not resolved, but spin-doubling does not collapse and is resolved. Accounting for the different partition functions and dipole moments, the abundance of the anion is found to be about 0.14% that of the neutral. Figure 3.3 shows the $J = 37 - 36$ absorption line of C_4H^-: a signal-to-noise ratio of 75 was achieved in only 25 minutes of integration, allowing line frequencies to be measured to $10 - 20$ kHz.

The detection of C_4H^- with the FTM spectrometer proved to be challenging. The anion was only detected in a discharge through diacetylene and when the buffer gas was He or H_2, the latter yielding the best signals. The anion-to-neutral ratio ranged from 1.2×10^{-3} with H_2 to an upper limit of 4×10^{-5} with Ne (Table 3.3). Further improvements in the production of C_4H^-, mainly by careful optimization of the composition of the gas discharge, have since been made and have been described in ref. [85].

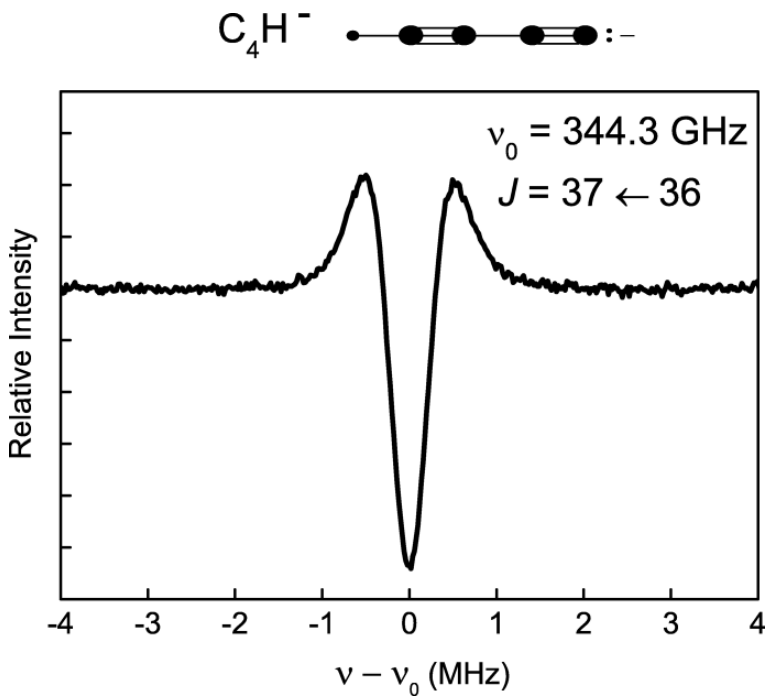

Figure 3.3: $J = 37 - 36$ transition of C_4H^- detected with the free space millimeter-wave spectrometer, after a 25 min integration. Owing to the modulation scheme used, the instrumental line shape is approximately the second derivative of a Lorentzian.

The initial search in the millimeter-wave band covered a frequency range of $\pm 0.15\%$ around three successive transitions ($J = 18-17, 19-18$, and $20-19$) predicted from the theoretical B. A single harmonic series of lines of comparable strength was found; narrowband searches yielded additional lines close to frequencies predicted on the basis of this limited data set. The two lowest transitions were then found with the FTM at frequencies extrapolated from the millimeter-wave data. Lines of C_4D^- [2] were detected at the isotopic

[2]These were detected in a discharge through DCCD/Ar in the free space spectrometer,

shift of 7.1%—nearly identical to that found for neutral C_4H.

Table 3.5: Measured rotational frequencies of C_4H^- and C_4D^- (in MHz).

	C_4H^-		C_4D^-	
$J' - J''$	Frequency	$O - C^a$	Frequency	$O - C^a$
$1 - 0$	9,309.887	−0.002		
$2 - 1$	18,619.758	−0.003	17,296.059	−0.006
$9 - 8$	83,787.263	−0.033		
$16 - 15$	148,948.610	−0.003		
$17 - 16$	158,256.620	0.037		
$18 - 17$	167,564.324	0.011		
$19 - 18$	176,871.783	−0.006		
$20 - 19$	186,179.030	0.033	172,945.149	0.007
$21 - 20$			181,590.734	0.021
$22 - 21$			190,236.061	0.023
$23 - 21$			198,881.115	0.011
$26 - 25$	242,015.829	0.000		
$27 - 26$	251,320.800	0.033		
$28 - 27$	260,625.328	0.004		
$29 - 28$	269,929.465	−0.021		
$30 - 29$			259,388.365	0.011
$31 - 30$	288,536.554	−0.015	268,030.922	0.003
$32 - 31$	297,839.465	0.003	276,673.102	−0.029
$33 - 32$			285,314.983	0.017
$37 - 36$	344,346.858	−0.016		
$38 - 37$	353,646.854	0.006		
$39 - 38$	362,946.288	0.003		
$41 - 40$			354,434.716	0.009
$42 - 41$			363,072.615	−0.016
$43 - 42$			371,710.056	−0.005

Note: Estimated 1σ uncertainties in line frequencies: 2 kHz in the centimeter-wave lines and 15 kHz in the millimeter-wave lines.
[a]Calculated from the spectroscopic constants in Table 3.4

Seventeen rotational transitions of C_4H^- and twelve of C_4D^- were measured to an accuracy approaching one part in 10^7 (Table 3.5). From the B

but only through a DC_4D/H_2 discharge in the FTM.

and D derived from these measurements, the radio spectrum of C_4H^- can now be calculated to better than 0.1 km s^{-1} in equivalent radial velocity through 800 GHz.

Additional evidence for C_4H^- was obtained by a direct determination of its charge by single pass measurements. Figure 3.4 shows the ion drift measurements of C_4H^-: the frequencies show the expected Doppler shifts when the polarity of the discharge is reversed. The sign of the shift is opposite to that observed for HCO^+, confirming that the carrier of the assigned lines in Table 3.5 is a negative ion.

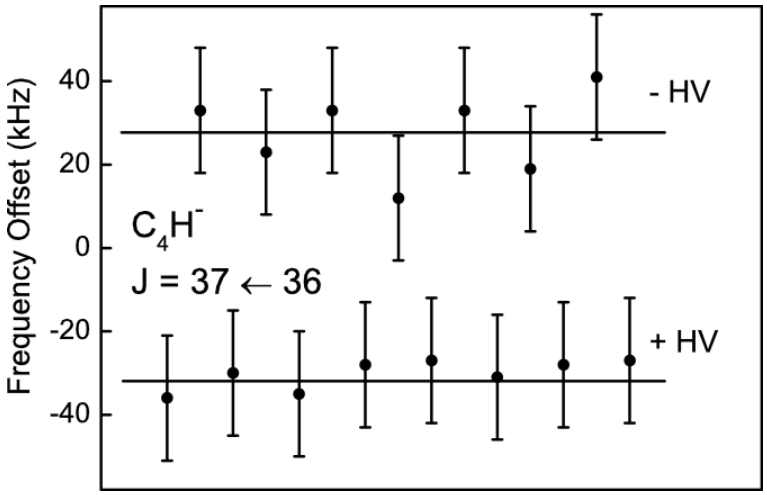

Figure 3.4: Ion drift of C_4H^-. Plotted here are a series of measurements for the $J = 37 \leftarrow 36$ line, in which either a positive or a negative high voltage (HV) applied to the electrode near the radiation source; in all cases, the electrode near the detector was grounded. The Doppler shift, relative to a center frequency of 344,346.874 MHz, corresponds to a drift velocity of 25 m s^{-1}.

3.3.2 C_6H^-

Because the spectroscopic constants of C_6H^- were known from astronomical observations, its detection required no search in frequency, but only optimization of the production conditions (Tables 3.2 and 3.3). Under favorable conditions, lines of C_6H^- in the millimeter-wave band were about 20 times weaker than those of C_6H, but were still observed with a signal-to-noise ratio of 10 or more in 1 hr of integration, allowing line frequencies to be measured to about 40 kHz or better. The line frequencies were unaffected by ion drift because the millimeter-wave radiation makes two opposite passes through the discharge cell. The concentration of C_6H^- in the glow discharge, corresponding to a mole fraction of 10^{-9}, was about 200 times less than that of C_6H (Table 3.2).

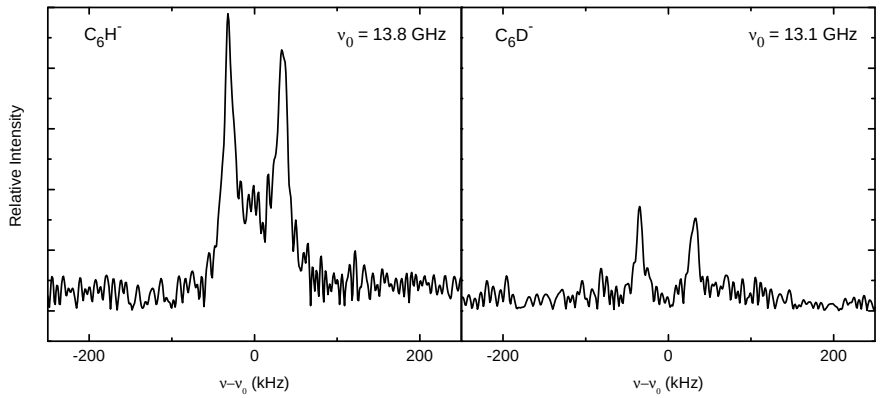

Figure 3.5: Rotational lines of C_6H^- and C_6D^-. The $J = 5 - 4$ transition of each species is shown; the integration time for each spectrum was about 30 min. See Fig 1.1 for an explanation of the observed line shape.

Rotational lines of C_6H^- in the centimeter-wave band were observed in a gas discharge through either acetylene or diacetylene heavily diluted with Ne. The lines are stronger in diacetylene, but because DCCD was readily available, that was the precursor used for producing C_6D^-. The strongest lines of C_6H^-, about 6 times weaker than those of C_6H observed under the same conditions, were detected with a signal-to-noise ratio of 20 in 20 minutes of integration. From a comparison of line intensities relative to those of the stable molecule OCS at a known fractional abundance (1% OCS in Ne), a density of about 10^8 C_6H^- per gas pulse—a few percent that of C_6H—was estimated.

Table 3.6: Measured rotational frequencies of C_6H^- and C_6D^- (in MHz).

	C_6H^-		C_6D^-	
$J' - J''$	Frequency	$O - C$	Frequency	$O - C$
$3 - 2$	8,261.174	0.000		
$4 - 3$	11,014.896	0.000	10,515.784	−0.001
$5 - 4$	13,768.612	−0.002	13,144.725	−0.001
$6 - 5$	16,522.329	0.001	15,773.660	0.000
$7 - 6$	19,276.038	0.001	18,402.593	0.003
$8 - 7$	22,029.740	−0.001	21,301.512	−0.002
$53 - 52$	145,928.242	0.030		
$54 - 53$	148,680.850	0.024		
$56 - 55$	154,185.988	0.059		
$57 - 56$	156,938.411	−0.005		
$58 - 57$	159,690.889	0.030		
$59 - 58$	162,443.214	−0.042		
$60 - 59$	165,195.588	−0.020		
$61 - 60$	167,947.947	0.034		
$62 - 61$	170,700.161	−0.009		
$64 - 63$	176,204.535	−0.006		
$68 - 67$	187,212.655	−0.023		

Note: Estimated 1σ uncertainties in line frequencies: 2 kHz in the centimeter-wave lines and $15 - 45$ kHz in the millimeter-wave lines.
[a]Calculated from the spectroscopic constants in Table 3.4

A total of 17 lines of C_6H^- and 5 of C_6D^- were measured to an accu-

racy approaching 0.1 ppm (see Table 3.7). One line each of the normal and deuterated species is shown in Figure 3.5: lines of C_6D^- were typically about 3 times weaker than those of C_6H^-, and were observed at precisely the expected deuterium shift of 4.53%—close to that observed for neutral C_6H (4.55%; [34]).

3.3.3 C_8H^-

The largest and most polar of the acetylenic anions studied here, C_8H^- was found only with the more sensitive FTM spectrometer. Under the best

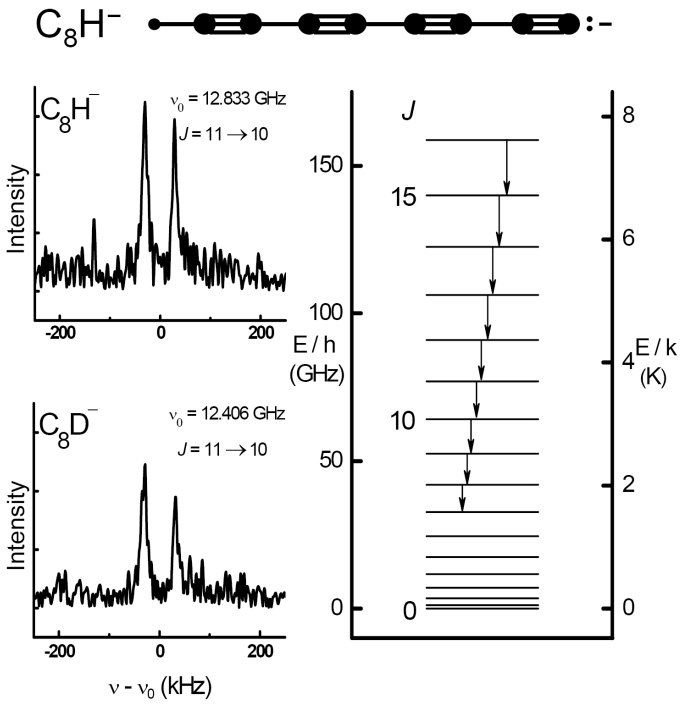

Figure 3.6: Rotational energy levels of C_8H^-, showing the transitions detected for the normal and deuterated isotopic species. *Top:* The geometrical structure of C_8H^-, the octatetrayne anion. *Left:* The $J = 11 - 10$ transition of each species, each obtained in 90 min integration.

conditions, the strongest lines of C_8H^- were observed with a signal-to-noise ratio of 10 in 90 minutes of integration (Fig. 3.6). The lines of C_8H^- are about 10 times weaker than those of C_8H observed under the same conditions, but are only a factor of $2-3$ weaker than those of C_6H^-. We estimate that there are about 10^8 C_8H^- molecules per gas pulse, which corresponds to about 2% that of C_8H—a similar ratio to that found for C_6H^- relative to C_6H.

Table 3.7: Measured rotational frequencies of C_8H^- and C_8D^- (in MHz).

	C_8H^-		C_8D^-	
$J'-J''$	Frequency	$O-C^a$	Frequency	$O-C^a$
$8-7$	9,333.434	0.001	9,022.528	−0.001
$9-8$	10,500.110	0.000	10,150.342	0.000
$10-9$	11,666.785	−0.001	11,278.156	0.001
$11-10$	12,833.460	0.000	12,405.967	0.000
$12-11$	14,000.134	0.000	13,533.778	0.000
$13-12$	15,166.806	0.000	14,661.589	0.001
$14-13$	16,333.476	−0.001	15,789.396	0.000
$15-14$	17,500.147	0.001	16,917.202	−0.002
$16-15$	18,666.814	0.000	18,045.010	0.001

Note: Estimated 1σ uncertainties in line frequencies are 2 kHz.
[a]Calculated from the spectroscopic constants in Table 3.4

Nine successive transitions of C_8H^- and nine of C_8D^- between 9 and 19 GHz were measured to an accuracy approaching 1 part in 10^7 (Table 3.7). Although the B and D are derived from measurements below 19 GHz, they are so accurately determined that the radio spectrum of C_8H^- can be calculated to well beyond the range of measurement: the uncertainty in equivalent radial velocity is less than 0.03 kms^{-1} at 20 GHz, and about 0.4 kms^{-1}—less than the line width in TMC-1 and IRC+10216, where this anion has now been detected. Similar to C_4D^- and C_6D^-, lines of C_8D^- were detected at the

expected isotopic shift of 3.3%.

3.3.4 C_3N^-

In contrast to the ease with which C_4H^- was detected with the free space spectrometer, the initial attempts to detect the isoelectronic ion C_3N^- were quite frustrating. It was only after two surveys[3] failed to yield evidence for C_3N^-, that a third search under different discharge conditions was successful[4]. The two changes that led to the detection of C_3N^- were: (i) the current of the glow discharge, was reduced to about 20 mA—$4-5$ times lower than that used in the first two searches; and (ii) commercial gases[5] were replaced by cyanoacetylene[6] (HC_3N, synthesized by the procedure described in Appendix B), because it had been shown that HC_3N best produces the C_3N radical [87] and that dissociative attachment to HC_3N at very low electron energies (1.6 eV; ref. [88]) produces the C_3N^- anion.

The density of background lines in the HC_3N discharge was quite high. In a typical spectrum there was 1 line every 10 MHz at an intensity comparable to that of C_3N^-, or roughly 50 background lines at each transition surveyed. Nevertheless lines of C_3N^- could be distinguished from the background, because transitions in the closed-shell $^1\Sigma$ electronic ground state are

[3]Each survey covered about 1.2 GHz of the millimeter-wave spectrum, and required about 10 hr of observation.

[4]The difficulties encountered have been discussed at length in ref. [78].

[5]The mixture used was (NCCN, 25%), acetylene (HCCH, 25%), and nitrogen (N_2, 50%), as it had yield strong lines of the C_3N radical.

[6]The composition of the gas mixture estimated from the flow rates was 20% HC_3N: 80% Ar (Appendix B).

closely harmonic in frequency and the theoretical centrifugal distortion constant (D; Table 2.3) was sufficiently accurate to allow prediction of successive transitions to within the pressure broadened linewidth (1.2 MHz). Two successive harmonically related lines at 262 and 272 GHz, tentatively assigned to the $J = 27 - 26$ and $28 - 27$ transitions, yielded a preliminary estimate of the rotational constant B. Additional lines with comparable intensities were then observed at both higher and lower frequencies confirming the assignment of C_3N^-. Figure 3.7 shows a line of C_3N^- near 339 GHz, along with the corresponding spin-doubled transition of C_3N which is about 100 times stronger under the optimum discharge conditions described above.

Table 3.8: Measured rotational frequencies of C_3N^-(in MHz).

	C_3N^-	
$J' - J''$	Frequency	$O - C^a$
$10 - 9$	97,028.656	−0.037
$12 - 11$	116,434.180	−0.003
$15 - 14$	145,539.368	−0.027
$16 - 15$	155,240.672	0.011
$19 - 18$	184,342.811	0.000
$23 - 22$	223,141.256	0.001
$25 - 24$	242,538.225	0.034
$27 - 26$	261,933.577	0.003
$28 - 27$	271,630.585	−0.008
$29 - 28$	281,327.147	−0.004
$35 - 34$	339,495.912	0.019
$39 - 38$	378,263.734	−0.016

Note: Estimated 1σ uncertainties in line frequencies are 15 kHz.
[a]Calculated from the spectroscopic constants in Table 3.4

Twelve rotational lines between 97 and 378 GHz have been measured,

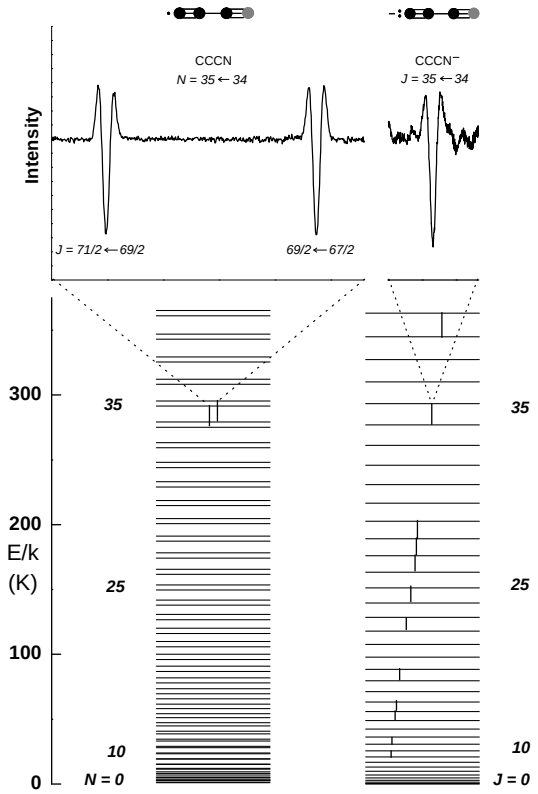

Figure 3.7: Sample laboratory spectra and rotational energy levels of C_3N and C_3N^-, illustrating the collapse of the spin doublet fine structure of C_3N on electron attachment. *Left:* $N = 35 \leftarrow 34$ transition of C_3N detected in an observation of 3 min, showing the well-resolved spin rotation doublets. The separations of the spin doublets are magnified 6000-fold on the energy level diagram. Frequency and Zeeman modulation were used simultaneously to remove background lines; the modulation scheme employed results in a lineshape that is approximately the second derivative of a Lorentzian. *Right:* Corresponding transition of C_3N^- detected in the same discharge after an observation of 10 min. The intensity scale is magnified relative to that of C_3N. The measured transitions are indicated by solid vertical lines.

and are summarized in Table 3.8. The B and D obtained from a least-squares fit to these data reproduce the observed frequencies to an rms of 19 kHz, comparable to the measurement uncertainty. From these constants the rotational spectrum of C_3N^- up to 500 GHz can be calculated to 0.03 kms^{-1} in radial velocity, adequate for deep searches even in sources which exhibit the sharpest molecular lines.

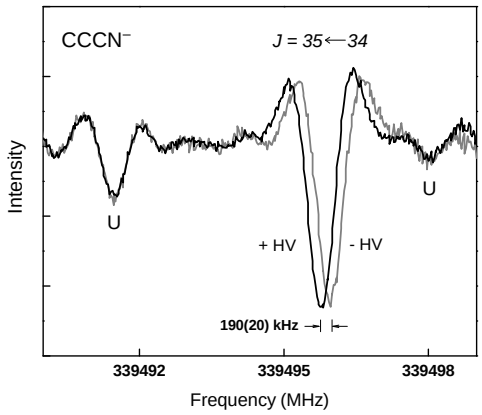

Figure 3.8: Ion drift measurement of C_3N^-. The $J = 35 \leftarrow 34$ absorption line of C_3N^- with either positive or negative high voltage (HV) applied to the electrode near the radiation source; the electrode near the detector was held at ground. The integration time for each spectrum was approximately 30 min. The frequency shift derived here (95 ± 10 kHz) corresponds to an axial ion drift velocity of 80 ± 10 m s^{-1}. The weak features marked U are from unassigned neutral molecules produced in the discharge.

As for C_4H^-, ion drift measurements have allowed direct determination of the charge of C_3N^-. As Figure 3.8 shows, a measurable Doppler shift in line frequency of the $J = 35 - 34$ transition was observed in the single-pass

arrangement. The sign of the shift changed in the expected direction when the discharge polarity was reversed, confirming that the observed line is from a negative ion. The observed drift velocity is within 10% of that derived from earlier measurements of CN^- in a similar discharge [77], on the assumption that the velocity is inversely proportional to the mass of the ion.

3.4 Discussion

The evidence supporting the identification of the carbon chain anions is extremely strong. Owing to the close structural similarity of the anions, essentially the same arguments can be used to assign with high confidence the observed lines to the individual anions. First, the anions are closed-shell linear molecules with $^1\Sigma$ ground states: the transitions are closely harmonic in frequency, separated by ratios of integer quantum numbers, and the lines lack the fine and hyperfine structure [7] characteristic of the neutral radicals, which have $^2\Sigma$ or $^2\Pi$ ground states, or that for the cations, which are either observed by optical spectroscopy or predicted *ab initio* to have triplet ground states. Second, the derived rotational constants agree remarkably well—generally to within 0.1%—with those calculated *ab initio*; and the small ratios of the centrifugal distortion constant to the rotational constant (D/B) are typical of linear carbon chains which behave like thin elastic rods with the same positive Young's modulus [89]. Third, the elemental composition of the discharge

[7] Quadrupole hyperfine structure from the ^{14}N nucleus is only observed in the lowest rotational transitions of the nitrile anions, CN^- and C_3N^-, and collapses rapidly with increasing values of J.

restricts the identity of the anion. Fourth, the spectra of the isotopically substituted anions, where available, are observed at precisely the expected isotopic shifts, confirming the assignments. Finally, by measuring the ion drift of two of the anions—C_4H^- and C_3N^-—it was possible to directly determine their charge, providing conclusive confirmation of the assignments.

Two spectroscopic factors resulting from electron attachment favor the detection of the linear anions. The radicals possess doublet electronic ground states, with fine and hyperfine structure and Λ-doubling from the unpaired electron, which spread the intensity of each transition across many lines. Electron attachment collapses this structure and simplifies the spectrum to that of a $^1\Sigma$ molecule, yielding lines that are 4–8 times [8] stronger per unit abundance—an effect which we dub "spectral compression". In addition, for the carbon chain anions CCH^- through C_8H^-, electron attachment also results in 1.5–7 times larger dipole moments, further increasing line intensities by 2–50 times. As Figure 3.9 shows, the net effect of spectral compression and increased polarity of the anions is to enhance the lines of the anion relative to those of the neutral radical by one to two orders of magnitude, with the smallest enhancement observed for C_6H^- and the largest for C_4H^-. This enhancement was a distinct benefit which was not originally anticipated.

The rotational constants of the four acetylenic anions are so accurately determined, that they allow accurate extrapolation to the rotational constant

[8] This factor depends on the temperature.

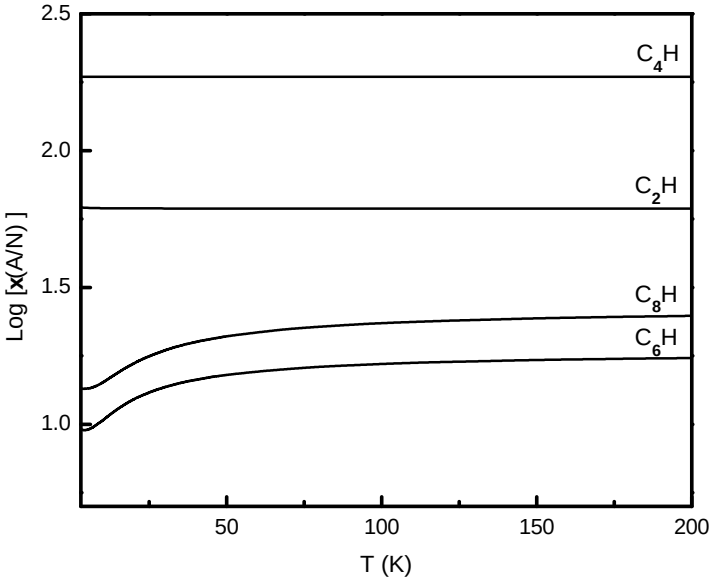

Figure 3.9: Enhancement (ξ) in the line intensity of the anion (A) relative to the corresponding neutral radical (N). Shown here is the ratio of the square of the dipole moments divided by the partition functions. The ratio is independent of temperature for CCH and C_4H owing to the $^2\Sigma$ ground state of the radicals, but it depends weakly on temperature for C_6H and C_8H in the $^2\Pi$ ground state.

of the next longer anion, $C_{10}H^-$. This was done by fitting a third-order polynomial to the moments of inertia of the shorter chains in the sequence (see, e.g., ref. [83]). The predicted rotational constant for $C_{10}H^-$ is 299.882(3) MHz, which is expected to be good to a few parts in 10^5 and from which the frequencies of lines near 10 GHz can be determined to within 50 kHz [9].

[9] A similar extrapolation of the the B of HC_9N from the rotational constants of the first four cyanopolyynes, HCN through HC_7N yields a value 290.5167 MHz, only 2 parts in 10^6 different from the measured value of 290.5183 MHz. The predicted frequency of

The formation of anions in both experiments is poorly understood. We consider first the glow discharge of our free space spectrometer, in which there are two possible routes for anion production: (i) radiative electron attachment (REA) to the radicals that are produced abundantly in the discharge, and (ii) dissociative electron attachment (DEA) to the precursor hydrocarbon to give the anion and hydrogen. Our experiments on C_3N^- may provide some indication as to which of the two processes is dominant in the glow discharge. The relative concentrations of C_3N^- and HC_3N were determined from measured line intensities under conditions that yielded the strongest lines of the anion. From these measurements, it appears that C_3N^- may be formed by DEA to HC_3N, because the C_3N^-/HC_3N ratio ($3 - 10 \times 10^{-6}$) is similar in discharges through different precursor gases, and C_3N^- was not observed in a discharge through NCCN and N_2 in which C_3N was produced but not HC_3N.

Next, we consider anion formation in the pulsed discharge of the supersonic nozzle of the FTM spectrometer referring to a recent study by McCarthy and Thaddeus [85]. The production of the anions relative to the neutral radicals is found to increase rapidly with chain length. While the C_4H^-/C_4H ratio is only 0.3%, the C_6H^-/C_6H and C_8H^-/C_8H ratios are $1\% - 2\%$ (Table 3.1). On the basis of the steep rise observed in the anion-to-neutral ratio from C_4H^- to C_6H^-—consistent with the theoretical conclusion of Herbst and coworkers [22, 90] that a critical size of six carbon atoms must be reached

the $J = 18 - 17$ transition is 10458.602 MHz, which is within 50 kHz of the measured 10458.639 MHz.

for efficient REA—McCarthy and Thaddeus conclude that anion formation in the supersonic nozzle likely proceeds *via* REA. They do not rule out DEA as a possible formation route, however, because recent experiments show that C_4H^- is produced from HC_4H at low electron energies, with a lower energetic threshold than for HCCH. Moreover, the C–H bond energies for HCCH and longer polyacetylenes are similar, indicating that C_4H^- could still form, albeit inefficiently, by DEA. If the threshold for anion formation decreases with chain length, larger anions might form more easily by the same process as well.

The formation of C_4H^- in the pulsed discharge requires highly specific conditions: the anion is only detected with diacetylene in either an H_2 or He buffer, and its formation is suppressed if more than 10% of Ne or Ar is added to the discharge [85]. The anion may be formed under these conditions, if electron attachment does not occur from C_4H in the $^2\Sigma$ ground which has a small dipole moment (0.87 D), but instead from the low-lying $^2\Pi$ state which is highly polar (4.5 D; see refs. [91–93]) and is thermally populated in the warmer He and H_2 expansions, but is not populated in the Ne or Ar expansions. The larger radicals C_6H and C_8H have $^2\Pi$ ground states with large dipole moments, which might explain the more efficient anion production relative to C_4H^-. A simpler explanation, however, may be that the residence times of the smaller anions C_4H^- and C_3N^- in the nozzle are shorter in beams of H_2 and He, which might mean that these anions are not destroyed as efficiently as in the slower beams of Ne or Ar (M. C. McCarthy, private communication).

Another observation concerning the formation of anions in the glow

disharge as well as in the supersonic nozzle, is that far lower currents—as much as 5 times lower—are required for the production of the anions. This might suggest that anions are destroyed by electron impact detachment [8,94], as the density and peak energy of electrons in the discharge increase with current. The increased availability of energetic electrons raises the probability of their collision with anions, leading to efficient destruction of the anions.

3.5 Conclusions

The accurate laboratory rest frequencies from this work have allowed sensitive radio astronomical searches for the relevant carbon chain anions. In fact, the spectroscopic constants derived from the laboratory data are so accurate, that the rotational spectra of these anions can be calculated throughout the radio band to within a fraction of the line width in nearly all astronomical sources. As discussed in the next chapter, of the four molecular anions that have now been observed in space, three have been conclusively identified on the basis of the laboratory data reported here.

The challenge now is to extend this work to a wider class of molecular anions, including nonlinear and planar ones, of interest to laboratory spectroscopists as well as astronomers. Particularly interesting are molecular anions with high binding energies, large dipole moments, and simple rotational spectra. Good candidates for laboratory detection include NCO^-, NCS^-, and $HCOO^-$, all of which have high binding energies ($\geq$ 3.5 eV), and for which high-level molecular structure calculations exist. Some anions of astrophysical

interest that may be detected with the present techniques are C_5N^-, CH_3CC^-, c-C_3H^-, H_2CCC^-, and H_2CCN^-. These cover a wide range in binding energy and dipole moment: C_5N^- and CH_3CC^- have large dipole moments, and binding energies that are comparable to those of C_6H^-, but the binding energies of the others are less than 2.0 eV. The rotational constants and leading centrifugal distortion constants of H_2CCC^-, and H_2CCN^- have been derived from autodetachment spectra [95], so the search for rotational lines may only require a fairly narrow frequency range.

Lines of neutral molecules in the glow discharge can overwhelm weaker ionic lines, frustrating the efforts to identify new molecular ions. Velocity modulation spectroscopy has been used with great success in infrared searches of ions, because it allows effective suppression of the background from neutral molecules, and at the same time discriminates between positive and negative ions because of the sign of the first-derivative lineshapes [82]. Implementation of this technique in the millimeter-wave band, however, is challenging at present, because ionic lines in the millimeter-wave band, as we have seen, are about 6 times weaker than those observed in the normal DC glow discharge. This is because the Doppler shift from the ion drift is typically less than one-third of the pressure-broadened line width—the shift is proportional to the frequency of the transition, as well as the electric field (see eq 3.1, ref. [82], and Fig 3.8). As noted in previous studies of molecular ions (see e.g., ref. [42]), the ion drift is sensitive to the experimental conditions. Enlarging the magnitude of the Doppler shift by a factor of 2 or so by some means, such as cooling

the cell or using different buffer gases would be a significant step towards enhancing velocity modulation. Alternatively, even a modest improvement, of about half an order of magnitude, in the sensitivity of the free space spectrometer, could make velocity modulation a viable technique in the millimeter-wave band, simplifying laboratory searches of new ions.

In addition to better detection sensitivity, improvements in anion production are highly desirable. That might be achieved through experimentation with different discharge configurations. The anions here were detected in the positive column of the normal DC glow discharge. Recently, however, "hollow anode" and extended negative glow discharges have also been shown to produce anions [41] at comparable abundances to that in the positive column. A systematic exploration of different types of discharges might yield conditions that enhance anion abundances, making detection of anions easier.

Chapter 4

Radio Astronomical Observations of C_4H^-, C_6H^-, C_8H^-, and C_3N^-

4.1 Introduction

The new laboratory results have given impetus to the search for molecular anions in the interstellar gas, starting with the identification of C_6H^-. With accurate rest frequencies in hand, deep radio astronomical searches have yielded detection of the related carbon chain anions C_4H^-, C_8H^-, and C_3N^-, all within the past three years. There is tentative evidence for the smaller anion, CCH^-, as well as for C_5N^-, which is isoelectronic with C_6H^-, but has not yet been detected in the laboratory. Table 4.1 is an overview, a summary of the radio astronomical references, and the frequency bands and sources in which the anions have been detected.

Here I discuss the astronomical observations of C_4H^-, C_6H^-, C_8H^-, and C_3N^- in the centimeter-wave band, done with the 100 m Green Bank Telescope (GBT), toward TMC-1. These observations have yielded detection of the two larger anions C_6H^- and C_8H^-, and upper limits on the abundances of the smaller anions C_4H^- and C_3N^-.

Table 4.1: Radio astronomical detections of carbon chain anions.

Molecule	Source	Frequency Range (GHz)	T_{rot} (K)	N (10^{10} cm^{-2})	A-N Ratio (%)	Telescope(s)[a]	Ref.
Confirmed:							
C_4H^-.....	IRC+10216	$83-140$	23(2)	70(20)	0.024	IRAM 30 m	[96]
	L1527	$83-140$	14	1.6	0.011	IRAM 30 m	[97]
C_6H^-.....	IRC+10216	$30-97$	32(3)	690(40)	8.6	NRO 45 m	[98]
	TMC-1	$8-14$	5	12(2)	1.6(3)	100 m GBT	[33, 76]
	L1527	$19-46$	10(5)	6(2)	10(3)	100 m GBT; NRO 45 m	[99]
	L1544	$19-20$	10	0.31(5)	2.5(8)	100 m GBT	[44]
	L1521F	$19-20$	10	0.34(7)	4(1)	100 m GBT	[44]
C_8H^-.....	TMC-1	$12-19$	5	2.1(4)	5(1)	100 m GBT	[76]
	IRC+10216	$28-45$	16(2)	260(40)	37	NRO 45 m	[100]
	IRC+10216	$25-45$	34	210	26	100 m GBT	[101]
C_3N^-.....	IRC+10216	$97-146$	29(2)	160(60)	0.5	IRAM 30 m	[78]
Tentative:							
C_2H^-.....	IRC+10216	$83-84$	...	...	0.008	IRAM 30 m	[55]
C_5N^-.....	IRC+10216	$83-140$	37(6)	340(120)	13-57	IRAM 30 m	[55]

[a] Abbreviations: IRAM–Institute de Radio Astronomie Millimetrique; NRO–Nobeyama Radio Observatory; GBT–Green Bank Telescope.

4.2 Observations

The observations were done in several sessions with the NRAO's 100 m GBT between 2006 July and 2007 October, as described in refs. [33, 76, 78]. Tables 4.2 and 4.3 list the observed transitions of C_6H^-, C_8H^-, C_4H^-, and C_3N^- as well as the corresponding neutral radicals. The frontends were Ku ($12-15.4$ GHz), K ($18-22.4$ GHz), and X-band ($8-10$ GHz) receivers, employing cooled HFET amplifiers [102]. Typical system temperatures were $25-35$ K in Ku-band, $30-40$ K in K-band, and $30-40$ K in X-band.

The backend, an autocorrelation spectrometer [102], was configured for simultaneous observations of both polarizations in four 50 MHz wide frequency windows, for a maximum resolution of 1.5 kHz (corresponding to the $32,768$ frequency channels of the spectrometer). Data from multiple sessions, as well

as the two polarizations were averaged and smoothed to a final resolution of 6.1 kHz to enhance the signal-to-noise ratio.

Spectra were acquired by position-switching with a period of 4 minutes, the OFF position lying 30″ east in right ascension of TMC-1. The pointing and focusing of the telescope were checked approximately every 90 minutes by observing a strong nearby continuum source (0431+2037); the pointing was generally good to 10″. Intensities at all frequencies were calibrated against the quasar 3C 147.

4.3 Analysis

Molecular column densities were derived[1] from the observed spectra based on the following assumptions: (i) the lines are optically thin; (ii) the source is much larger than the telescope beam; and (iv) the population of rotational energy levels is described by a single rotational temperature, T_{rot}. The total column density (N_T) of a molecule is then given by

$$N_T \;=\; N_J \left(\frac{Z}{g_J}\right) \;\exp\; \left(\frac{E_J}{kT_{rot}}\right), \tag{4.1}$$

where J is the angular momentum quantum number of the upper level, N_J is the population of the level, g_J is the degeneracy of the level, E_J the energy of the level, and Z the rotational partition function.

In the Rayleigh-Jeans approximation, the following expression relates

[1]The derivation follows that given in the Appendix of ref. [103]

N_J to the integrated intensity W of an optically thin line:

$$N_J \;=\; \frac{T_{rot}}{T_{rot}-T_{bg}}\;\frac{g_J 3kW}{8\pi^3\nu S\mu_x^2} \tag{4.2}$$

where $W \equiv \int T_R dv$ is the integrated intensity, T_{bg} is the background brightness temperature, S is the line strength of the transition, ν the frequency (in GHz), and μ_x is the dipole moment (in D) along a principal axis of inertia. Combining equations (4.1) and (4.2) yields

$$N_T \;=\; \frac{T_{rot}}{T_{rot}-T_{bg}}\;\frac{3kZ\int T_R\,dv}{8\pi^3\nu S\mu_x^2}\;\exp\left(\frac{E_J}{kT_{rot}}\right). \tag{4.3}$$

When $T_{rot} >> T_{bg}$, i.e., the contribution from the background is negligible, equation (4.3) simplifies to

$$N_T \;=\; \frac{3kZ\int T_R\,dv}{8\pi^3\nu S\mu_x^2}\;\exp\left(\frac{E_J}{kT_{rot}}\right). \tag{4.4}$$

The column densities reported in this chapter were evaluated using eq. (4.3), since a low T_{rot} of 5 K was assumed. Those in Chapter 5 were calculated using eq. (4.4), as the T_{rot} used there were higher than 10 K.

4.4 Results

4.4.1 C_6H^- and C_8H^-

The observations of C_6H^- in TMC-1 have been discussed in Chapter 1 (see Figure 1.1). The $J = 4 - 3$ and $J = 5 - 4$ transitions of C_6H^- detected toward TMC-1 in 2006 July with the 100 m GBT along with the same transitions observed with our FTM spectrometer are shown in Fig. 1.1. Following

these observations a third transition, the $J = 3 - 2$ line, was subsequently detected in TMC-1 (Table 4.2), resulting in a revision in the column density of C_6H^-. In addition, the column density of C_6H[2] was derived from new observations with the GBT, which resulted in a slight change in the C_6H^-/C_6H ratio in TMC-1: from 2.5% to 1.6% (Table 4.3).

Table 4.2: Lines of C_6H^-, C_6H, C_8H^-, and C_8H in TMC-1.

	Transition			Frequency	T_A^*	V_{LSR}	Δv
Molecule	$J' - J$	$F' - F$	Parity	(MHz)	(mK)	(km s^{-1})	(km s^{-1})
C_6H^- [a]	$3 - 2$	···	···	8,261.174	13(1)	···	0.41(5)
	$4 - 3$	···	···	11,014.896	25(3)	5.80(2)	0.38(4)
	$5 - 4$	···	···	13,768.612	41(2)	5.80(11)	0.33(2)
C_6H [b]	$7/2 - 5/2$	$4 - 3$	e	9,703.498	71(3)	···	0.40(2)
		$3 - 2$	e	9,703.609	61(4)	···	0.30(2)
		$4 - 3$	f	9,703.834	66(3)	···	0.45(3)
		$3 - 2$	f	9,703.945	66(3)	···	0.45(3)
	$11/2 - 9/2$	$6 - 5$	e	15,248.247	214(4)	···	0.39(1)
		$5 - 4$	e	15,248.322	169(4)	···	0.39(12)
		$6 - 5$	f	15,249.084	206(4)	···	0.36(1)
		$5 - 4$	f	15,249.158	189(4)	···	0.37(1)
	$13/2 - 11/2$	$7 - 6$	e	18,020.574	278(13)	···	0.34(3)
		$6 - 5$	e	18,020.644	231(13)	···	0.30(3)
		$7 - 6$	f	18,020.818	267(13)	···	0.33(2)
		$6 - 5$	f	18,021.752	241(14)	···	0.29(2)
	$15/2 - 13/2$	$8 - 7$	e	20,792.872	187(8)	···	0.37(2)
		$7 - 6$	e	20,792.945	170(7)	···	0.37(2)
		$8 - 7$	f	20,794.444	194(7)	···	0.38(2)
		$7 - 6$	f	20,794.512	176(8)	···	0.34(2)
C_8H^- [c]	$11 - 10$	···	···	12,833.460	8(1)	5.71(5)	0.36(4)
	$12 - 11$	···	···	14,000.134	7(1)	5.86(5)	0.37(4)
	$13 - 12$	···	···	15,166.806	6(1)	5.84(6)	0.45(4)
	$16 - 15$	···	···	18,666.814	10(2)	5.80(7)	0.34(5)
C_8H [a]	$25/2 - 23/2$	···	e	14,666.686	···	···	···
		···	f	14,666.771	···	···	···

Notes: Line parameters are derived from a least-squares fit of gaussian profiles to the spectral lines. The coordinates of TMC-1 are $\alpha(1950) = 04^h38^m38.6^s$, $\delta(1950) = +25°35'45.0''$.
[a]The frequencies are from ref. [33]. [b]Frequencies from ref. [105]; e/f denote the Λ-doublet parity. [c]Frequencies from ref. [75] [d]Frequencies from ref. [105]; e/f denote the Λ-doublet parity, and the hfs is only partially resolved. The integrated area was obtained from spectra shown in Fig. 4.2.

[2]The initial estimate was somewhat uncertain, because it was derived from observations of C_6H with the NRAO 43 m telescope [104].

Figure 4.1 summarizes the observations of C_8H^-. As shown, four rotational transitions have been detected at a modest signal-to-noise ratio (about 3) achieved in nearly 40 hours of integration. The identification is free from anomalies: the velocities, widths, and relative intensities (see Table 4.3) of the lines are those expected for TMC-1; the velocities and widths match well those of other molecules in this source (e.g., HC_9N, shown at the bottom of Fig. 4.1). The low density of lines in TMC-1 and the apparent absence of blends enhance considerably the confidence in the identification of C_8H^-.

Lines of C_8H^-, like those of C_6H^-, are stronger than might be expected in space owing to the smaller partition function and the larger dipole moment relative to those of C_8H. As Fig. 4.2 shows, the C_8H^- lines are only about 3 times weaker than one of the hyperfine components of C_8H, although C_8H is about 20 times more abundant. The large gain in line intensity results from spectral compression: the intensity spread over several lines in the open-shell radical because of fine and hyperfine structure and Λ-doubling collapses into a single line of the closed-shell anion. The nearly twofold larger dipole moment of the anion enhances the line intensities by nearly a factor of 4, enhancing detection in the radio band.

The column densities (N_T) of the carbon chain anions and their parent neutral radicals are summarized in Table 4.4, along with the dipole moments

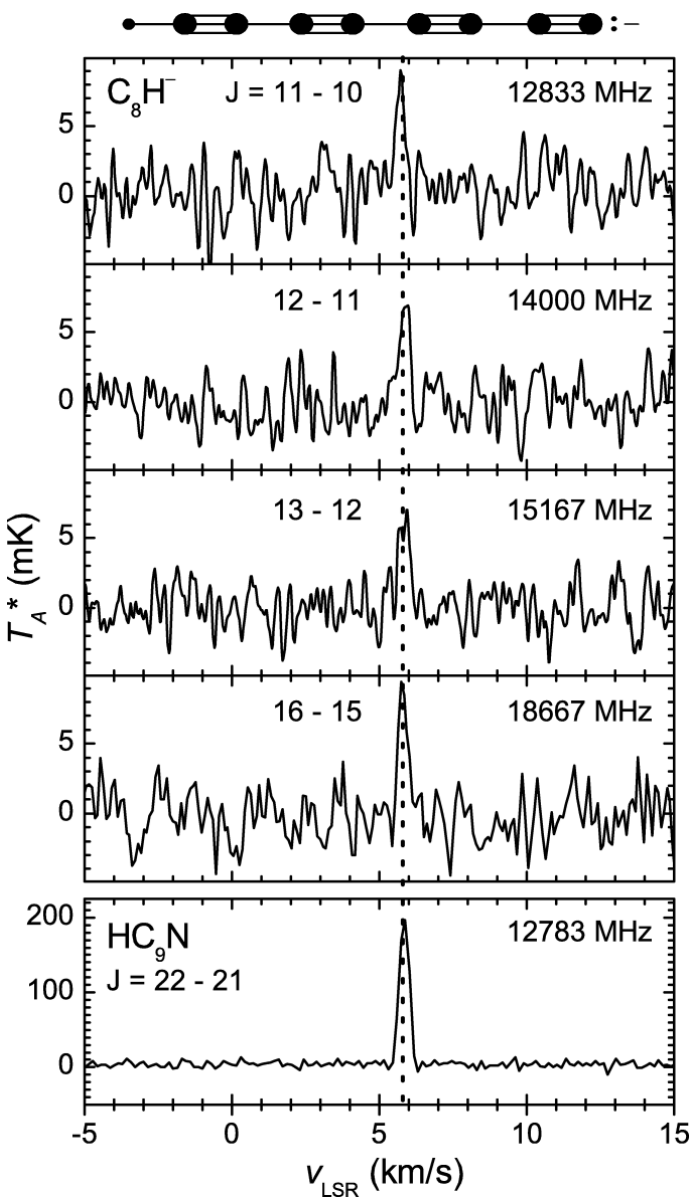

Figure 4.1: Observed lines of C_8H^- in TMC-1 and one of HC_9N for comparison (*bottom*). The dashed line is at $v_{\rm LSR} = 5.8$ km s^{-1}, the assumed source velocity. The spectra are smoothed to a resolution of 6.1 kHz. Data from several observing sessions and from both polarizations were averaged to improve the signal-to-noise ratio. The total integration time for the C_8H^- lines was about 37 hr in *Ku*-Band and about 27 hr in *K*-Band.

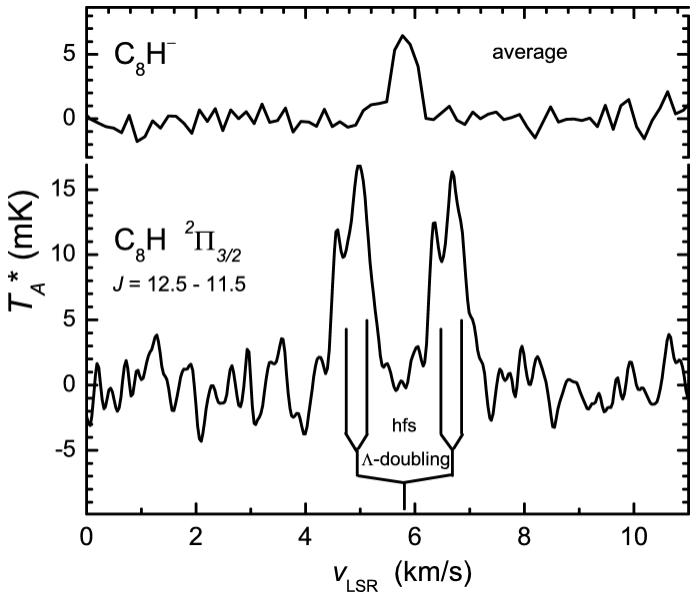

Figure 4.2: Spectral compression in C_8H^-. *Top:* average of the four lines of C_8H^- in TMC-1; *bottom:* Lines of the indicated transition of C_8H, showing well-resolved Λ-doubling and partially-resolved hyperfine structure. The spectra have been smoothed to a resolution of 6.1 kHz.

and partition functions (Z) used in our calculations. The relevant line parameters are given in Tables 4.2 and 4.3. Because the observed transitions are few and arise from levels that are fairly close in energy, it was not feasible to extract a rotational temperature from the data; in the analysis a rotational temperature of 5 K was assumed—the value obtained by Bell et al. [104] from observations of C_6H with the NRAO 43 m telescope. Although the C_6H and C_8H radicals had been observed previously, three transitions of C_6H and one of C_8H were re-observed (Table 4.2) to minimize uncertainties caused by different telescope beams.

4.4.2 C_4H^- and C_3N^-

The shorter carbon chain C_4H^- and the isoelectronic C_3N^- were not detected in TMC-1. The upper limit of the C_4H^-/C_4H ratio ($< 0.004\%$) is nearly three orders of magnitude lower than the observed C_6H^-/C_6H and C_8H^-/C_8H ratios, and is nearly 5 times smaller than that observed in IRC+10216 ($<$ 0.02% Ref. [96]). The upper limit of the C_3N^-/C_3N ratio in TMC-1, however, is comparable to the observed ratio in IRC+10216 (0.52%; Ref. [78]). The much lower limit of the anion-to-neutral ratio for C_4H compared with that of C_3N is because lines of C_4H are several times more intense than those of C_3N in TMC-1 and the spectroscopic enhancement for C_4H^- (100; Ref. [75]) is about 40 times larger than for C_3N^- (2.4; Ref. [78]).

4.5 Discussion

The larger anions, C_6H^- and C_8H^-, are present in TMC-1 at fractional abundances of a few percent relative to their parent radicals. This indicates that the anions are formed by a simple and efficient mechanism. A likely process is radiative electron attachment (REA): $A + e^- \leftarrow A^- + h\nu$, which is favored by a large electron affinity of the radical, and a high density of vibronic states, which allows rapid relaxation to the ground state of the anion [22]. Both C_6H and C_8H possess high EAs (3.8 and 4.0 eV, respectively [40]) and are large by the standards of astronomical molecules. The threefold greater

Table 4.3: Observed Line Parameters of C_4H and C_3N and Upper Limits of C_4H^- and C_3N^- in TMC-1.

	Transition			Frequency	T_A^*	V_{LSR}	Δv
Molecule	$N' - N$	$J' - J$	$F' - F$	(MHz)	(mK)	(km s^{-1})	(km s^{-1})
C_4H^- [a]	$1 - 0$	···	···	9,309.887	< 8	···	···
	$2 - 1$	···	···	18,619.758	< 7	···	···
C_4H [b]	$1 - 0$	$3/2 - 1/2$	$1 - 0$	9,493.060	186(7)	5.67	0.33(2)
	···	···	$2 - 1$	9,497.615	605(11)	5.64	0.31(7)
	···	···	$1 - 1$	9,508.005	162(7)	5.61	0.31(7)
C_3N^- [c]	$1 - 0$	···	$2 - 1$	9,703.406	< 21	···	···
	$2 - 1$	···	$3 - 2$	19,406.536	< 12	···	···
C_3N [d]	$2 - 1$	$5/2 - 3/2$	$5/2 - 3/2$	19,780.808	203(9)	5.72	0.25(1)
	···	···	$3/2 - 1/2$	19,780.823	128(9)	5.54	0.21(2)
	···	···	$5/2 - 5/2$	19,781.005	47(7)	5.83	0.35(6)
	···	···	$7/2 - 5/2$	19,781.090	344(9)	5.56	0.24(7)
	···	···	$3/2 - 3/2$	19,783.537	56(10)	5.62	0.16(3)
	···	$3/2 - 1/2$	$3/2 - 3/2$	19,797.472	59(8)	5.62	0.23(4)
	···	···	$3/2 - 1/2$	19,799.959	71(7)	5.69	0.26(3)
	···	···	$5/2 - 3/2$	19,800.126	205(8)	5.69	0.25(1)
	···	···	$1/2 - 1/2$	19,800.971	65(7)	5.65	0.27(3)

Notes: Line parameters are derived from a least-squares fit of gaussian profiles to the spectra. The coordinates of TMC-1 are $\alpha(1950) = 04^h38^m38.6^s$, $\delta(1950) = +25°35'45.0''$.
[a] The frequencies are from ref. [75]. [b] Frequencies from refs. [87,106] [c] Frequencies from ref. [78]. [d] Frequencies from unpublished FTM measurements in a supersonic molecular beam (estimated 1σ uncertainties 5 kHz).

C_8H^-/C_8H ratio compared with the C_6H^-/C_6H ratio is plausibly the result of the higher density of states in the larger radical. The abundances of the C_6H^- and C_8H^- recently predicted by Millar et al. [90] are in good agreement with our observed values, suggesting that REA may indeed be the main route to anion formation.

Chemical models, however, fail to reproduce the observed C_4H^-/C_4H ratio, which is lower by at least two orders of magnitude than that calculated. The C_4H radical also has a large EA and is only somewhat smaller than C_6H, so the surprisingly low limit for C_4H^-/C_4H suggests that other factors may be important in anion formation. A marked difference between C_4H and the two larger radicals is its polarity: only 0.9 D versus 5.5 and 6.3 D for C_6H

and C_8H, repectively. As discussed in the literature (see e.g., [107], [108]), the cross-sections for electron attachment increase rapidly with dipole moment, and take on large values for molecules with dipole moments greater than about 2.5 D, owing plausibly to the existence of dipole-bound states (DBS) that may facilitate anion formation. Because of its small dipole moment and the absence of a DBS supported by its electronic ground state [92], electron capture and the formation of a temporary negative ion—the first steps in REA [109]—may be highly inefficient for C_4H. The high C_4H^-/C_4H ratio of 1% calculated by Millar et al. [90] might therefore be at best an upper limit, since their model assumes that a temporary negative ion is formed upon each collision with an electron.

Table 4.4: Abundances of Carbon Chain Anions and Radicals in TMC-1.

Molecule	Dipole Moment[a] (D)	Z(5 K)	N_T (10^{10}cm^{-2})	Anion-to-neutral Ratio (%)
C_8H^-	11.9	179	2.1(4)	5(1)
C_8H	6.3	720	46(4)	···
C_6H^-	8.2	76	12(2)	1.6(3)
C_6H	5.5	312	750(80)	···
C_4H^-	6.2	23	< 2.3	< 0.004
C_4H	0.9	89	61000(5000)	···
C_3N^-	3.1	128	< 70	< 0.8
C_3N	2.9	65	9500(500)	···

[a]Values for C_4H^- and C_6H^- are from ref. [24], for C_4H and C_6H from ref. [110], for C_8H^- from ref. [75], and for C_8H from ref. [111].

Detection of the isoelectronic C_3N^- in TMC-1 may clarify the role of the dipole moment in electron attachment and anion formation. The C_3N

radical has a larger EA (4.6 eV [88]) than C_4H, and is similar in size, but its dipole moment is more than three times larger—large enough to support a DBS (2.9 D [91])—implying that electron attachment, and hence anion formation may be much more efficient, and therefore C_3N^-/C_3N may be much higher than C_4H^-/C_4H. This might explain the observations in IRC+10216, where C_3N^-/C_3N is found to be about 20 times greater than C_4H^-/C_4H ([78]; see also, Table 4.1), although dissociative electron attachment (DEA) to HNC_3 is also thought to contribute to the production of C_3N^- there [78].

4.6 Conclusions

Because lines of the anions are weak, and require long integration for detection—e.g., C_8H^- was detected after 40 hours of observation—the prospect of finding still larger anions might seem poor. This conclusion may be overly pessimistic, however, given that larger anions can form even more efficiently than smaller ones. The longer chain $C_{10}H^-$ is extremely polar with a dipole moment of nearly 16 D [70] compared with 7.5 D for $C_{10}H$; in addition, it has a larger binding energy [24] than C_8H^-. Its high polarity and spectral compression make $C_{10}H^-$ a good candidate for astronomical detection, as the lines of the anion are expected to be stronger than those of the neutral if the $C_{10}H^-/C_{10}H$ ratio exceeds about 30%—quite possible, because a comparably large ratio, of about $30-40\%$ has been observed for C_8H^- [100, 101]. If so, 10 carbon atoms would be a 'cross-over' point in the series of linear carbon chains, at which the anions are more conspicuous than the radicals.

Detection of more exotic anions may shed some light on anion formation and related processes in space. Finding the asymmetric rotor CH_2CN^-, for example, might clarify the role of electron affinity in the formation of anions, because the neutral parent radical, which is abundant in many sources (e.g., [112]), has a large dipole moment (3.5 D) but a fairly small electron affinity (1.5 eV; [40]). Similarly, the detection of the three-membered ring c-C_3H^- and its bent-chain isomer l-C_3H^- may help explain the relative abundances of the cyclic and linear forms of neutral C_3H in different molecular sources. The c-C_3H/l-C_3H ratio is about 10 in the cold dark cloud TMC-1, whereas the same ratio is nearly an order of magnitude lower in the warm molecular shell of IRC+10216. To explain this, the process of electron catalyzed isomerization has been invoked: collisions of slow electrons with l-C_3H yield l-C_3H^-, which rearranges to the more stable c-C_3H^-; autodetachment from c-C_3H^- then yields c-C_3H [113]. If so, observations of the anions of C_3H could help test the validity of this mechanism.

The astronomical detection of four anions in a fairly short time suggests that negative ions may be more widely distributed and easier to observe than previously supposed. Many other anions probably exist in space, and their rotational spectra may be detectable with large, sensitive telescopes like the GBT. As the lines of anions are generally weak, however, high-resoultion laboratory data are an important prerequisite for deep searches for these molecules in space.

Chapter 5

A Survey of C_4H, C_6H, and C_6H^- with the Green Bank Telescope

5.1 Introduction

Molecular anions were identified only recently [1] in the two well-studied sources, IRC+10216 and TMC-1. More recently, C_6H^- was detected in the low-mass star forming region L1527 [99]. In all three sources, C_6H^- was found at surprisingly high abundances relative to C_6H.

As an inspection of Table 4.1 shows, C_6H^- is the most readily observed molecular anion in astronomical sources, plausibly because C_6H is small enough to be produced at fairly high abundances in molecular clouds, but large enough for efficient electron attachment [118]. In the known sources of anions, lines of C_6H^- are several times stronger than those of all other molecular anions [76,78,96,100,101]. However, better anion sources probably exist in space and await detection. A search for C_6H^- in a wide variety of galactic molecular sources, was a logical step in the astronomical study of molecular anions

[1] Molecular cations, however, have been known since the beginning of molecular astronomy, with CH^+ among the first three molecules detected in the interstellar gas [114]. The two most widely distributed molecular cations, HCO^+ and N_2H^+, have been used to study the physical and chemical conditions in many astronomical sources [115–117].

To determine the distribution of molecular anions in space and to better establish their abundance relative to that of their neutral counterparts, a survey of C_6H^- with the 100 m Green Bank Telescope toward 24 galactic molecular sources was recently undertaken. Although the main purpose of this survey was to find new sources of C_6H^-, in the process the related carbon chain radicals, C_4H and C_6H were surveyed as well. Here I present the results of this survey, including the detections of C_4H and C_6H in several new sources, and of C_6H^- in two new dark clouds.

5.2 Observations

The observations were done with the NRAO's 100 m GBT; the specifications are summarized in Table 5.1. The main survey consisted of simultaneous observations of lines of C_4H, C_6H, and C_6H^- between $18 - 22$ GHz with the K-band receiver, but a few observations were done between $8 - 10$ GHz with the X-band receiver during poor weather. Another search was done for C_6H^- in two sources, Sgr B2(N) and W51 (M/S), with the Ku-band, but C_6H was not searched for at Ku-band as these observations were done prior to the identification of C_6H^-.

The observing procedure was essentially the same as that described in the previous chapter and in ref. [76]. Spectra were taken by position switching, with a frequency resolution across a 50 MHz band in narrow line sources or a 200 MHz band in wide line sources, as summarized in Table 5.1. At all frequencies, two orthogonal polarizations were observed simultaneously and

Table 5.1: GBT Specifications.

ν (GHz)	η	$\Delta\nu$ (kHz)	$T_{\rm sys}$ (K)	Date
$8-10$	0.94	1.5, 6.1	$20-35$	2008 April–May
$12-15.4$	0.92	24.4	$20-35$	2006 July
$18-22.4$	0.86	1.5, 6.1	$30-60$	2008 April–May
$\cdots$		24.4	$30-60$	2008 April–May

Note: Beam diameter = $740/\nu$ (FWHM), η is the telescope beam efficiency, $\Delta\nu$ is the resolution, and T_{sys} is the total system temperature including constribution from the earth's atmosphere.

averaged to improve the signal-to-noise ratio.

Where strong lines of C_4H were detected, we made a 5-point map of the C_4H emission to ensure that the maximum emission from the larger carbon chains was sampled[2]. The map was made by moving the telescope beam $30''$ east, west, north, and south with respect to the central position and integrating for 8 min at each point. One such map, that of L1544, is shown in Appendix D.

Of the 24 sources covered in the survey, half are dark clouds; the rest include translucent and diffuse clouds, photon-dominated regions (PDRs), low mass protostars, giant molecular clouds associated with HII regions, and circumstellar envelopes of carbon-rich stars (see Table 5.2). Nine were selected because of prior evidence of C_4H, and two of C_6H; others known to contain HC_3N and larger cyanopolyynes, but not necessarily carbon chain radicals, were also included.

[2]This is observed, for example, at the cyanopolyyne peak of TMC-1

Table 5.2: Source List.

Source	α(1950)	δ(1950)	Ref.
Dark Clouds:			
Barnard 1[a]	03 30 10.5	+30 57 47	[119]
L1495B[b]	04 12 35.3	+28 40 19	[120]
L1521B[a,b]	04 21 10.5	+26 30 00	[120]
IRAM04191+1522[a]	04 24 47.6	+15 36 36	[121]
L1521F[a]	04 25 35.0	+26 44 60	[122]
L1521E[b]	04 26 12.5	+26 07 17	[123]
L1551[a]	04 28 40.0	+18 01 42	[124]
L1512	05 00 54.4	+32 39 00	[122, 125]
L1544[b]	05 01 12.3	+25 06 40	[122]
L183[b]	15 51 32.7	−02 39 30	[122]
L1082A[a]	20 52 20.1	+60 03 14	[126]
L1251[a]	22 37 51.5	+74 55 50	[126]
Translucent and Diffuse Clouds:			
CB17(L1389)[a,b]	04 00 36.0	+56 47 59	[127, 128]
B0415+379 (3C111)	04 15 01.5	+37 54 07	[129, 130]
Photon Dominated Region:			
Horsehead Nebula[b,c]	05 38 23.4	−02 29 29	[131]
Low Mass Protostars:			
NGC1333-2A	03 25 50.9	+31 04 18	[132, 133]
NGC1333-4A	03 26 05.0	+31 03 13	[132, 133]
Giant Molecular Clouds:			
W3 (HCN)	02 21 47.0	+61 52 54	[134]
Sgr B2(N)	17 44 10.0	−28 21 15	[135]
W51 (M/S)	19 21 26.3	+14 24 35	[135]
Carbon Rich Circumstellar Envelopes:			
CRL618[b]	04 39 33.8	+36 01 15	[136]
CIT6	10 13 11.0	+30 49 17	[136]
CRL2688[b,c]	21 00 20.0	+36 29 44	[136–138]
CRL3068	23 16 42.4	+16 55 10	[136]

Notes. Units: right ascension (α) in hours, minutes, and seconds; declination (δ) in degrees, arcminutes, and arcseconds.
[a]Source contains a low-mass protostellar object observed either in IRAS or *Spitzer* IR surveys.
[b]Indicates previous detection of C_4H.
[c]Previous detection of C_6H.

5.3 Results

The survey results toward dark clouds are given in § 5.3.1, those toward L1544 and L1521F are described in § 5.3.1.1, and trends in the abundances of carbon chains in § 5.3.1.2. Results for representative molecular sources other than dark clouds are summarized in § 5.3.2. The intensities, widths,

and velocities of the observed lines are listed in Tables C.1 and 5.3. Derived column densities and abundance ratios are summarized in Table 5.4.

5.3.1 Dark Clouds

Twelve dark clouds—eight in the Taurus complex—were observed in the present survey. Large carbon chain radicals had previously been observed in only a few: C_4H in 10 (of which 5 are covered here) and C_6H in 2 (TMC–1 and L1527). Here, C_4H was detected in 11 dark clouds and C_6H in 5. In many of these, lines of C_4H are moderately intense ($T_A > 100$ mK), and in some, only $2-5$ times weaker than those in TMC–1 (Fig. 5.3a). Where C_6H is detected, its lines are only about $2-6$ times weaker than those in TMC–1, and as Fig. 5.4 shows, the column density $N(C_6H)$ is linearly related to $N(C_4H)$.

Two sources in Taurus—L1544 and L1521F—show strong lines of C_4H and C_6H, and it is in these that the carbon chain anion C_6H^- was detected (Figs. 5.1 and 5.2). The new detections double the number of dark clouds where C_6H^- is known. In a few other dark clouds, where lines of C_6H are comparable in strength to those in L1544 and L1521F, C_6H^- may be close to detection (e.g., there is a hint of a weak line, about 10 mK, in L1521B after 8 hours of observation).

5.3.1.1 L1544 and L1521F

L1544 is one of best known examples of a prestellar core apparently close to gravitational collapse, while L1521F has recently been found to contain

a very low luminosity protostar [122, 139]. Single antenna and interferometric observations of N_2H^+, N_2D^+, $C^{18}O$, CS, and CCS and millimeter-wave dust continuum observations toward both sources reveal several features associated with the earliest stages of low-mass star formation: (i) a high degree of CO depletion; (ii) dense (10^6 cm^{-3}) cores surrounded by extended lower density ($\sim 10^4 - 10^5$ cm^{-3}) gas; (iii) evidence for gravitational infall from the widths and asymmetric velocity profiles of molecular lines; and (iv) enhanced deuterium fractionation as indicated by the large N_2D^+/N_2H^+ ratio [122, 140–144].

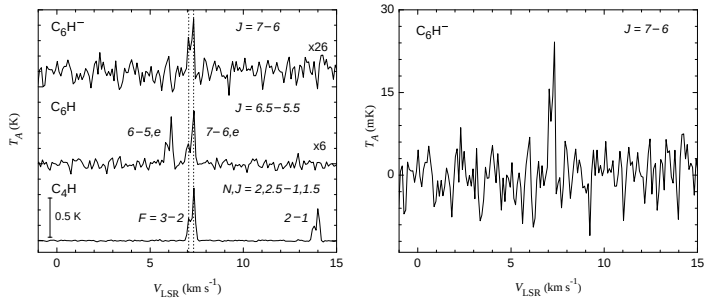

Figure 5.1: Line profiles of C_6H^-, C_6H, and C_6H toward L1544. *Left:* Spectra of C_6H^-, C_6H, and C_4H showing similar velocity structure in all three species. Lines of C_6H^- and C_6H have been scaled to the peak intensity of the C_4H line; the dashed lines are at velocities of 7.1 and 7.35 km s^{-1}. *Right:* Blow-up of C_6H^-. Spectra are smoothed to a resolution of 6.1 kHz. The total integration time is 10 hr for C_6H^-, and 4 hr for C_6H and C_4H.

Double-peaked line profiles of C_4H, C_6H, and C_6H^- were detected toward the peak N_2D^+ emission in L1544. The partially resolved peaks are quite narrow,[3] with a weak component at 7.1 km s^{-1} and a stronger one at

[3]The observed line widths are only about $1.5-2$ times larger than the thermal line width

7.35 km s^{-1} (Fig. 5.1). The observed doubling is not hyperfine structure, because the separation between the two components ($\sim$0.25 km s^{-1}) is much smaller than the hyperfine splitting in C_4H and C_6H (see Fig. 5.1 and Table 5.4), and because fine and hyperfine structure is absent in the closed-shell C_6H^- [33]. The relative intensities of the two velocity components are reversed with respect to those of other molecular lines (e.g., N_2D^+ and N_2H^+; [143]). Because the lines of all three carbon chains are almost certainly optically thin, the observed asymmetry is unlikely to result from self-absorption; it is more likely caused by a spatial asymmetry in the source, with more red-shifted than blue-shifted gas, the dip in the center resulting from freeze-out of long carbon chains in the core of L1544 (P.C. Myers, private communication).

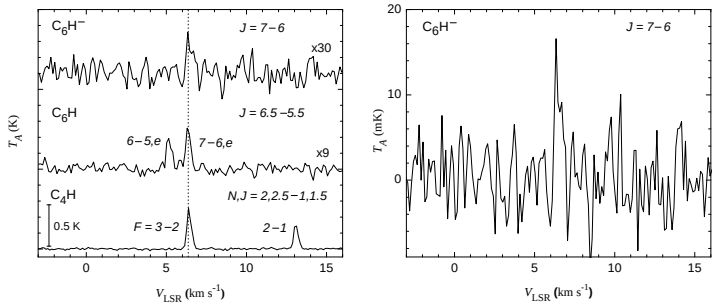

Figure 5.2: Line profiles of C_6H^-, C_6H, and C_6H in L1521F. *Left:* Spectra of C_6H^-, C_6H, and C_4H showing unresolved asymmetric lines which peak at a velocity of 6.4 km s^{-1} (dashed line). Lines of C_6H^- and C_6H have been scaled to the peak intensity of the C_4H line. *Right:* Blow-up of C_6H^-. Spectra are smoothed to a resolution of 7.5 kHz. The total integration time is 10 hr for lines of C_6H^- and C_6H and 2 hr for C_4H.

of 0.1 km s^{-1} (FWHM) at 10 K.

Lines of C_4H, C_6H, and C_6H^- were also detected near the peak emission of N_2D^+ in L1521F (Fig. 5.2). As shown in the left-hand panel of Fig. 5.2, the line profiles of C_4H, C_6H, and C_6H^- are asymmetric, but do not show well-resolved velocity structure like that toward L1544, possibly because of the more complex structure of this source [144]. The asymmetric profiles observed here are similar to those found for HC_5N [145].

5.3.1.2 Relative Abundances of Carbon Chains

For simplicity, we define R_N as the C_6H/C_4H ratio and R_A as C_6H^-/C_6H. Five trends are apparent in the dark clouds surveyed here: (i) R_N lies approximately between that observed in L1527 and TMC–1 ($0.2 - 1\%$; Fig. 5.3b); (ii) R_A is similar to that in TMC–1 and L1527 ($1 - 10\%$; Fig. 5.3c); (iii) R_N approaches that in TMC–1 in only two sources (L1495B and L1521B), (iv) R_A does not exceed that of L1527, and (v) The highest observed R_N is in L1495B and R_A in L1521F; the lowest observed R_N is in L1521F and R_A in L1544.

5.3.2 Other sources

In sources other than dark clouds, C_4H and C_6H were detected in only two: the translucent cloud CB17 and the carbon star CRL2688); C_6H^- was not detected in any. In CB17, R_N is about 1% and $R_A < 4\%$, similar to that in dark clouds. The upper limit of R_A in CRL2688 (23%) is nearly three times larger than that found in IRC+10216 (8.6%; [98]). The three species were not detected in the Horsehead nebula, where C_4H and C_6H have previously been

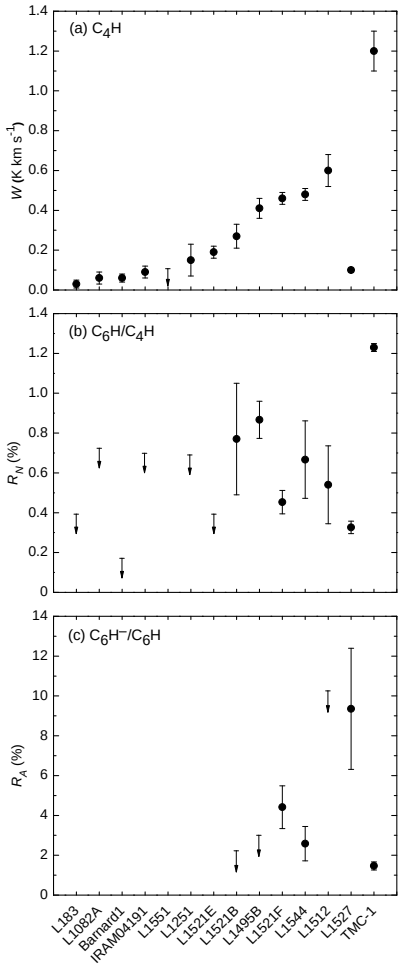

Figure 5.3: Comparison of C_4H, C_6H, and C_6H^- in dark clouds. (a) Velocity integrated intensity ($W = \int T_A dv$) of the $N = 2 - 1$ lines of C_4H; data for L183 and Barnard 1 have been scaled from observations of the $N = 1 - 0$ lines, and for L1527 from the $N = 9 - 8$ lines; (b) the C_6H/C_4H ratio (R_N); and (c) the C_6H^-/C_6H ratio (R_A). See Table 4.1 for references to the data in TMC-1 and L1527.

reported in the 3 millimeter-wave band [97, 131].

Table 5.3: Observed Line Parameters.

	C_4H				C_6H				C_6H^-			
Source	T_A	v_{LSR}	Δv	$\int T_A dv$	T_A	v_{LSR}	Δv	$\int T_A dv$	T_A	v_{LSR}	Δv	$\int T_A dv$
Dark Clouds:												
L1512	455(7)	7.14(3)	0.15(2)	0.60(8)	60(12)	7.12(3)	0.10(2)	0.04(1)	< 47	···	0.15	< 0.007
L1521B	372(11)	6.32(3)	0.17(3)	0.27(6)	40(6)	6.53(3)	0.32(5)	0.06(2)	< 14	···	0.2	< 0.003
	232(13)	6.53(3)	0.13(3)									
L1495B	590(20)	7.67(3)	0.26(3)	0.41(5)	130(20)	7.62(4)	0.23(3)	0.11(1)	< 30	···	0.25	< 0.008
L183	90(10)	2.30(4)	0.26(3)	0.03(2)	< 50	···	···	< 0.015	< 63	···	0.3	< 0.019
Barnard1	20(4)	6.49(4)	1.4(3)	0.06(2)	< 8	···	1.5	< 0.013	< 11	···	1.5	< 0.016
L1521E	240(20)	6.77(3)	0.26(3)	0.19(3)	< 72	···	0.3	< 0.022	< 42	···	···	< 0.013
IRAM04191+1522	90(10)	6.68(3)	0.32(5)	0.09(3)	< 60	···	0.3	< 0.02	< 40	···	0.3	< 0.014
L1082A	50(10)	2.12(7)	0.3(1)	0.06(3)	< 60	···	0.3	< 0.012	< 50	···	0.3	< 0.01
L1551	< 50	···	0.5	< 0.104	< 50	···	0.5	< 0.03	< 40	···	0.5	< 0.02
L1251	48(8)	−3.48(6)	0.7(1)	0.15(8)	< 50	···	1.0	< 0.05	< 33	···	1.0	< 0.04
Translucent and Diffuse Clouds:												
CB17(L1389)	160(10)	−4.73(3)	0.30(3)	0.15(2)	18(5)	−4.77(5)	0.30(5)	0.02(1)	< 0.023	···	0.3	< 0.007
3C111	< 14	···	2	< 0.03	< 15	···	2	< 0.03	< 11	···	2	< 0.022
Photon Dominated Region:												
Horsehead Nebula	< 13	···	0.7	< 0.01	< 13	···	0.7	< 0.01	< 17	···	0.7	< 0.012
Low Mass Protostars:												
NGC1333-2A	< 15	···	5	< 0.075	< 16	···	5	< 0.08	< 14	···	5	< 0.07
NGC1333-4A	< 13	···	5	< 0.065	< 18	···	5	< 0.09	< 13	···	5	< 0.065
Giant Molecular Clouds:												
W3(HCN)	< 8	···	5	< 0.04	< 12	···	5	< 0.06	< 10	···	5	< 0.05
Sgr B2(N)	< 6	···	20	< 0.12								
W51 (M/S)	< 7	···	15	< 0.11								
Carbon Rich Circumstellar Envelopes:												
CRL618	< 7	···	15	< 0.11	< 12	···	15	< 0.18	< 8	···	15	< 0.12
CIT6	< 7	···	25	< 0.18	< 8	···	25	< 0.20	< 9	···	25	< 0.23
CRL2688	9(1)	−33(1)	29(2)	0.41(4)	4(1)	−33(1)	29(2)	0.11(5)	< 3	···	30	< 0.09
CRL3068	< 5	···	24	< 0.13	< 6	···	24	< 0.15	< 6	···	24	< 0.15

Note.—Units: T_A in mK, v_{LSR} and Δv in km s^{-1}, and $\int T_A dv$ in K km s^{-1}. Line parameters derived from least-squares fits of Gaussian profiles to observed spectra. For C_4H and C_6H, $\int T_A dv$ has been summed over all fine and hyperfine components. Except where noted lines were observed in the $18 - 22$ GHz band. See Table 4 for line parameters in L1544 and L1521F. Peak intensity of the strongest hyperfine component of C_4H ($N, J, F = 2, 2.5, 3 - 1, 1.5, 2$) at 19,015.144 MHz. Peak intensity of the strongest hyperfine component of C_6H ($^2\Pi_{3/2}, J = 6.5 - 5.5, F = 7 - 6, e$) at 18,020.574 MHz. From observations in $8 - 10$ GHz band. See ref. [76] for rest frequencies. From observations in $12 - 15$ GHz band. Rest frequency for C_6H^- is 13,768.612 MHz [33].

Table 5.4: Column densities and abundance ratios.

Source	$T_{\rm rot}^{a}$ (K)	$N(C_4H)$ (10^{13} cm^{-2})	$N(C_6H)$ (10^{11} cm^{-2})	$N(C_6H^-)$ (10^{9} cm^{-2})	R_N (%)	R_A (%)
L1544	10	18(6)	12(3)	31(5)	0.7(2)	2.5(8)
L1521F	10	17(3)	8(1)	34(7)	0.45(6)	4(1)
L1512	10	9(3)	5(2)	< 48	0.5(2)	< 11
L1521B	10	10(2)	8(3)	< 17	0.8(3)	< 2.2
L1495B	10	15(5)	13(1)	< 310	0.9(1)	< 2.4
L183	10	3(2)	< 4.3	< 120	< 0.39	···
Barnard 1	10	7(6)	< 1.3	< 97	< 0.18	···
L1521E	10	7(3)	< 2.7	< 66	< 0.39	···
IRAM04191+1522	10	3(1)	< 2.3	< 52	< 0.70	···
L1082A	10	2(1)	< 1.5	< 48	< 0.71	···
L1551	10	< 4	< 3.2	< 98	< 0.82	···
L1251	10	5(3)	< 3.7	< 190	< 0.69	···
CB17(L1389)	10	5(2)	6(3)	< 25	1.2(8)	< 4.2
B0415+379 (3C111)	30	< 3	< 9	< 9	···	···
Horsehead Nebula	15	< 2	< 250	< 4.3	···	···
NGC1333-2A	50	< 1.2	< 39	< 1300	···	···
NGC1333-4A	50	< 1	< 44	< 1200	···	···
W3(HCN)	30	< 4.1	< 18	< 600	···	···
SgrB2N	30		< 2600	···	···	···
W51 M/S	30		< 2200	···	···	···
CRL618	90	< 33	< 140	< 4000	···	···
CIT6	13	< 18	< 56	< 2800	···	···
CRL2688	25	35(4)	45(1)	< 1000	1.3(2)	< 23
CRL3068	17	< 8	< 40	< 1700	···	···

Note: Column densities were calculated (see ref. [103]) from the velocity integrated intensities ($\int T_A dv$) in Tables 5.2 and 5.3, and corrected for beam efficiencies given in Table 5.1. Assumed dipole moments: 8.2 D for C_6H^- [24]; 0.9 D for C_4H and 5.5 D for C_6H [110]. [a]Assumed rotational temperature (see references in Table 5.1).

5.4 Discussion

As might be expected from the close structural similarity, the column densities of C_6H and C_4H in cold dark clouds are closely linked (Fig. 5.4).

A similar correlation between HC_3N and HC_5N, and between and these two molecules and C_4H was previously observed by Federman et al. (1990; [146]), who found that the ratio $N(HC_3N)/N(HC_5N) \approx 3$ holds for a sample of 22 dark clouds, and concluded that long carbon chains are probably formed by similar processes, e.g., addition of acetylenic (C_2) units to form larger chains [147, 148]. Our data probably indicate a similar connection between C_4H and C_6H, with $N(C_4H)/N(C_6H) \approx 100$ (or $R_N \approx 0.01$) in dark clouds. Detection of C_4H and C_6H in a larger sample of dark clouds than that surveyed here would be required to better constrain this ratio. More empirical studies such as the one here and that by Federman et al. are needed to critically evaluate chemical models of the chemistry of dark clouds.

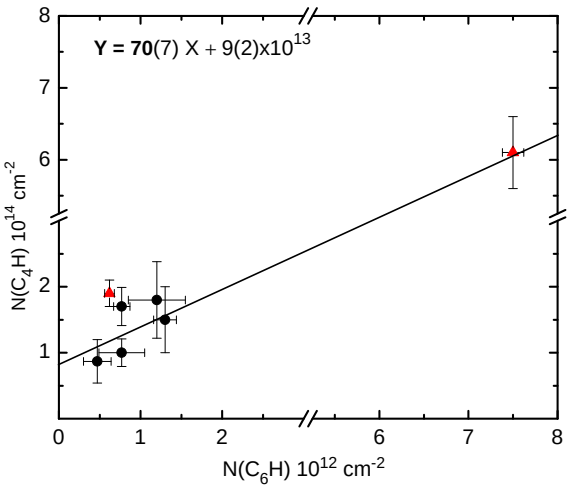

Figure 5.4: Correlation between the column densities of C_6H and C_4H in dark clouds. Black circles indicate data from this survey, and red triangles those for TMC-1 (top) and L1527 (bottom).

There have been several published chemical model calculations of carbon chain abundances in TMC-1—the cold dark cloud that has received the most observational and theoretical attention. In a recent time-dependent model optimized for TMC-1 [90], the column densities of C_6H and C_4H are too low by a factor of 3 and 13, respectively, and R_N is too low by a factor of 4. Better agreement for the calculated R_N could be attained at longer assumed times (i.e., $> 3.16 \times 10^5$ yr), but the column densities would then be much too low. Owing to the large uncertainties in the calculated abundances of C_4H and C_6H, it is not feasible to infer the ages of dark clouds and to make detailed comparisons of the chemistry of different clouds on the basis of current time-dependent chemical models and the measurements reported here.

The calculated abundances of anions are even more uncertain than those of the corresponding neutral species, because as noted by Millar et al. (2007; [90]) the rates for radiative electron attachment ($A + e \rightarrow A^- + h\nu$), and the product distributions (branching ratios) of subsequent reactions of molecular anions with atomic species have not been measured in the laboratory. Although the calculated R_A for TMC-1 is only about three times higher than that observed [76], the calculated C_4H^-/C_4H ratio is at least $10 - 100$ times too high [78, 118]. A detailed quantitative comparison of the calculated abundances of C_4H, C_6H, and C_6H^- with those in Table 5.4, awaits laboratory measurements of the rates of formation and destruction of these carbon chain radicals and anions.

The C_6H^- anion may be close to detection in at least three other

dark clouds studied here. The R_A in TMC–1, L1544, and L1521F is similar (Fig. 5.3c), indicating that C_6H^- might be detectable in clouds where the column density of C_6H [$N(C_6H)$] is comparable to these representative sources. In three clouds—L1521B, L1495B, and L1512—R_N and $N(C_6H)$ are comparable to those in L1544 and L1521F (Fig. 5.3a and Table 5). For example, in L1521B the upper limit of $N(C_6H^-)$ (corresponding to R_A ~2%) is at least a factor of 3 lower than the other dark clouds in Table 5, suggesting that C_6H^- may be detectable in a few other sources, especially L1495B and L1512, with only 3 to 4 times deeper integration. If sources with R_A comparable to that of L1527 are found ($\sim$ 10%; [99]), then C_6H^- might be detectable even if lines of C_6H are weak.

Detection of C_6H^- toward other sources may be possible with deeper searches. Lines of C_6H in CRL2688 near 20 GHz are fairly weak ($<$ 5 mK), so detection of the anion in this frequency band would require a nine fold deeper integration if R_A is comparable to that in IRC+10216. Because CRL2688 is a fairly warm source ($25 < T_{rot} < 80$ K), searches for transitions in the millimeter-wave band from levels near the peak of the Boltzmann distribution might yield detection of C_6H^-. In CB17, our upper limit for R_A of 4% is only slightly greater than that observed in dark clouds, but lines of C_6H are quite weak ($\sim$ 20 mK; see Table 4). If R_A is similar to that for the three representative dark clouds (L1544, L1521F, and TMC–1), then C_6H^- might be detectable in CB17 with $40 - 50$ hours of integration.

The fairly narrow range of R_A (Fig. 5.3c) might reflect differences in

the rate of production of C_6H^- in the four known dark clouds. As shown by Flower et al. [149], the electron abundance varies as $n^{1/2}$, whereas the H abundance is predicted to be independent of the density [150]. Hence, the observed variation in R_A may reflect differences in the electron abundances in these sources. In L1544, L1521F, and TMC–1 ($n \sim 10^4 - 10^5$ cm^{-3}) R_A is $1 - 4\%$, while in L1527 ($n \sim 10^6$ cm^{-3}) R_A is $3 - 5$ times higher, consistent with the higher estimated density ([99]; see Appendix E).

The anion-to-neutral ratio may yield a fairly direct measure of the electron density in dark clouds. We illustrate this by an approximate calculation of $[e]/[H_2]$ from the observed R_A, the rate of electron attachment (k_{ra}) to C_6H, and the abundance of atomic hydrogen (see Appendix E). For L1544 and L1521F, our estimate of the fractional ionization from a single point measurement of $10^{-8} - 10^{-7}$, is somewhat higher than that obtained from extensive measurements and analysis of N_2D^+ and N_2H^+ ([143,144]), but closer to that derived from observations of CO, HCO^+, and DCO^+ toward low-mass cores. The two main sources of uncertainty are k_{ra}, and the abundance of H. Laboratory measurements of k_{ra} as well as possible improved estimates of the H abundance in dark clouds (e.g., ref. [151]) may allow tighter constraints on the fractional ionization derived from molecular anions.

5.5 Conclusions

This survey has resulted in an increase in the number of known galactic sources of C_4H by nearly 50%, and C_6H by more than two fold. Although only

a few molecular clouds have been surveyed for large carbon chain radicals, our results for dark clouds indicate that the abundance of C_6H may be closely tied to that of C_4H. Here, C_4H was observed in nearly all dark clouds, and C_6H in those which showed strong lines of C_4H, indicating that C_4H may be a useful surrogate for large carbon chains in future surveys. Indeed, a recent survey of seven dark clouds in the southern sky has found moderate to strong lines of C_4H in six sources [152]. The brightest of these sources—B228[4] in the Lupus nebula—shows more intense C_4H emission than toward L1527 where C_6H and C_6H^- have both been detected [99]. A search for C_6H and C_6H^- is now underway, and it is probable that the two are detected in B228 as well (N. Sakai, private communication).

Studies similar to those done here could be extended to other free radicals and their anions: C_3N and C_5N are natural choices, as they are isoelectronic with the acetylenic radicals. A survey of C_3N, followed by searches for C_5N in sources that show strong lines of the former would help elucidate the chemistry of these radicals, and should serve as a starting point for the deep surveys of their anions. As modern telescopes generally allow simultaneous observations of four or more frequency bands, these searches could be undertaken simultaneously as well.

The two new sources of C_6H^- found here increase nearly twofold the number of sources accessible to the study of molecular anions, and more may

[4]IRAS15398 − 3359

be found in similar surveys. Some promising sources yet to be studied include dark clouds in the Aquila rift, e.g., L492, where large cyanopolyynes are as abundant as in TMC–1 [153], and the carbon star IRAS 15194-5115, where C_4H is three times more abundant than in IRC+10216 [154]. In future observations, the larger carbon chain C_8H^- should be surveyed as well, because larger anions are formed more efficiently, and it is possible that these are found more readily than smaller ones.

The results here lead one to strongly suspect that molecular anions may be close to detection in many astronomical sources—in dark clouds especially, but in other sources as well. Owing to simplicity of their production (see Appendix E), molecular anions may be widespread here as well as in other galaxies. Although this survey failed to find better sources of anions than those known previously, there is good reason to be optimistic about the prospect of finding such sources.

There are precedents for molecules which have been detected with difficulty at first, but which have turned out to be ubiquitous in space. A fine example is H_3^+—the molecule that plays a central role in the ion-molecule chemistry [155] of space: this important cation was found in the interstellar gas only after repeated attempts spanning 16 years since its detection in the laboratory [156]. In the three years since its identification, C_6H^- has already been found in five sources. We speculate that it is quite probable that surveys covering a significantly larger fraction of the sky than explored thus far for emission from large molecules, accompanied by even a modest increase in

the sensitivity of existing telescopes, will find molecular anions in many more interstellar and circumstellar sources.

Appendices

Appendix A

Harmonic Frequencies and Vibration-Rotation Interaction Constants

Table A.1: Harmonic vibrational frequencies and vibration-rotation interaction constants[a].

	Molecule				
	C_2H^-	C_4H^-	C_6H^-	CN^-	C_3N^-
ω_1	3372	3510	3506	2071	228
ω_2	1842	2156	2219		560
ω_3	536	1952	2118		885
ω_4		888	1952		1990
ω_5		698	1168		2247
ω_6		491	661		
ω_7		247	622		
ω_8			575		
ω_9			529		
ω_{10}			271		
ω_{11}			109		
α_1	294.8	6.8	0.9	249	26.2
α_2	302.4	22.9	5.0		19.2
α_3	−229.1	15.3	3.3		12.2
α_4		10.5	2.7		−16.0
α_5		−7.6	2.9		−32.4
α_6		−12.8	−2.6		
α_7		−23.4	1.3		
α_8			−2.4		
α_9			−3.4		
α_{10}			−4.5		
α_{11}			5.2		

[a]Basis sets: for the carbon chain anions, the cc-pCVQZ basis set was used for C_2H^-, and cc-pVTZ for the larger anions; the aug-cc-pCV5Z basis set was used for CN^-, and the aug-cc-pVQZ for C_3N^-; throughout, all electrons were correlated.
[b]Bonds are numbered starting at the terminal C atom for the acetylenic anions, and at the terminal N atom for the nitrile anions.

Appendix B

Synthesis of Cyanoacetylene

Cyanoacetylene (HC_3N) was synthesized 20 g at a time with a yield of about 70% by a procedure similar to that described in ref. [157]. To ensure a high yield of propiolamide ($HCCCONH_2$, the product of the first step in the synthesis), the large excess of NH_3 was removed by flushing the reaction vessel with N_2 and bubbling it through concentrated HCl. Methanol (CH_3OH), a by-product of the reaction, was then pumped away. The sample was stored indefinitely at -20° C with no discernible evidence of polymerization, but during the experiment HC_3N was held at a slightly higher temperature (-10° C) to provide sufficient vapor pressure (P(mm) $\sim$60 torr; [158]). A flow rate of $3-4$ cm^3 min^{-1}, estimated with a mass flow controller, yielded near optimum line intensities of the C_3N radical and a reasonable rate of HC_3N consumption of approximately 0.5 g h^{-1}. In most experiments here the flow of HC_3N vapor was maintained with a manual metering valve, because in a few days running the electronic flow controller becomes clogged. Consequently the flow rate of HC_3N is less certain than that of the other precursor gases, owing to changes in the vapor pressure resulting from variations in the sample bath temperature.

Appendix C

Lines in L1544 and L1521F

Table C.1: Lines observed toward L1544 and L1521F.

Transition $F' - F$	T_A (mK)	$v_{\rm LSR}$ (km s^{-1})	Δv (km s^{-1})	$\int T_A dv$ (K km s^{-1})
		L1544		
		C_4H		
		$(J = 2.5 - 1.5)$		
$2 - 1$	209(3)	7.09(3)	0.18(3)	0.11(2)
	453(4)	7.34(3)	0.15(3)	···
$3 - 2$	310(3)	7.10(3)	0.20(3)	0.18(3)
	678(4)	7.35(3)	0.15(3)	···
$2 - 2$	27(2)	7.08(4)	0.22(3)	0.015(3)
	60(2)	7.34(4)	0.14(1)	···
		$(J = 1.5 - 0.5)$		
$1 - 1$	44(3)	7.09(4)	0.19(3)	0.019(3)
	71(3)	7.37(3)	0.15(1)	···
$2 - 1$	200(3)	7.09(3)	0.20(3)	0.12(2)
	435(4)	7.34(3)	0.15(1)	···
$3 - 2$	93(3)	7.07(4)	0.19(3)	0.045(7)
	175(4)	7.34(3)	0.15(1)	···
		C_6H		
$7 - 6, e$	42(3)	7.03(3)	0.21(2)	0.028(3)
	113(3)	7.32(3)	0.16(2)	···
$6 - 5, e$	49(3)	7.07(3)	0.18(14)	0.023(3)
	95(3)	7.34(3)	0.14(1)	···
$7 - 6, f$	48(4)	7.07(3)	0.15(1)	0.025(3)
	114(4)	7.36(4)	0.14(2)	···
$6 - 5, f$	41(4)	7.05(4)	0.30(4)	0.025(3)
	88(4)	7.30(3)	0.13(1)	···
		C_6H^-		
	16(2)	7.08(3)	0.16(3)	0.0060(12)
	26(2)	7.30(3)	0.13(3)	···
		L1521F		
		C_4H		
		$(J = 2.5 - 1.5)$		
$2 - 1$	209(3)	6.38(3)	0.25(3)	0.11(1)
	453(4)	6.60(3)	0.21(3)	···
$3 - 2$	506(5)	6.39(3)	0.26(3)	0.17(2)
	148(8)	6.63(3)	0.21(3)	···
$2 - 2$	52(3)	6.38(4)	0.29(3)	0.018(2)
	12(3)	6.65(5)	0.15(8)	···
		$(J = 1.5 - 0.5)$		
$1 - 1$	108(8)	6.32(3)	0.28(3)	0.040(5)

Continued on next page ...

	55(7)	6.54(5)	0.22(5)	···
$2-1$	305(4)	6.39(3)	0.28(3)	0.11(1)
	72(3)	6.63(3)	0.19(3)	···
$3-2$	66(3)	6.38(3)	0.20(4)	0.019(1)
	26(4)	6.63(6)	0.15(8)	···
		C_6H		
$7-6, e$	58(3)	6.34(3)	0.30(2)	0.020(3)
	14(3)	6.59(5)	0.13(2)	···
$6-5, e$	44(3)	6.30(3)	0.23(4)	0.016(3)
	25(3)	6.55(3)	0.22(3)	···
$7-6, f$	53(4)	6.38(4)	0.24(1)	0.015(3)
	10(4)	6.64(4)	0.15(2)	···
$6-5, f$	37(4)	6.27(5)	0.30(4)	0.011(3)
	13(4)	6.33(5)	0.13(1)	···
		C_6H^-		
	17(2)	6.33(5)	0.18(3)	0.007(1)
	9(2)	6.64(5)	0.35(9)	···

Notes: Rest frequencies in MHz (see Gottlieb et al. 1983; McCarthy et al. 1999, 2006).

C_6H^- ($J = 7-6$): 19,276.038 MHz;

C_4H ($N, J = 2, 2.5-1, 1.5$): 19,014.720 ($F = 2-1$), 19,015.144 ($3-2$), and 19,025.107 ($2-2$);

C_4H ($N, J = 2, 1.5-1, 0.5$): 19,044.760 ($1-1$), 19,054.476 ($2-1$), and 19,055.947 ($3-2$);

C_6H ($^2\Pi_{3/2}, J = 6.5-5.5$): 18020.574 ($F = 7-6, \Lambda$-component e), 18020.644 ($F = 6-5, e$), 18021.752 ($F = 7-6, f$), and 18021.818 ($F = 6-5, f$).

Line parameters derived from least-squares fit of two Gaussian profiles to spectra shown in Figs. 3 and 4.

Appendix D

Five-point Map of C_4H in L1544

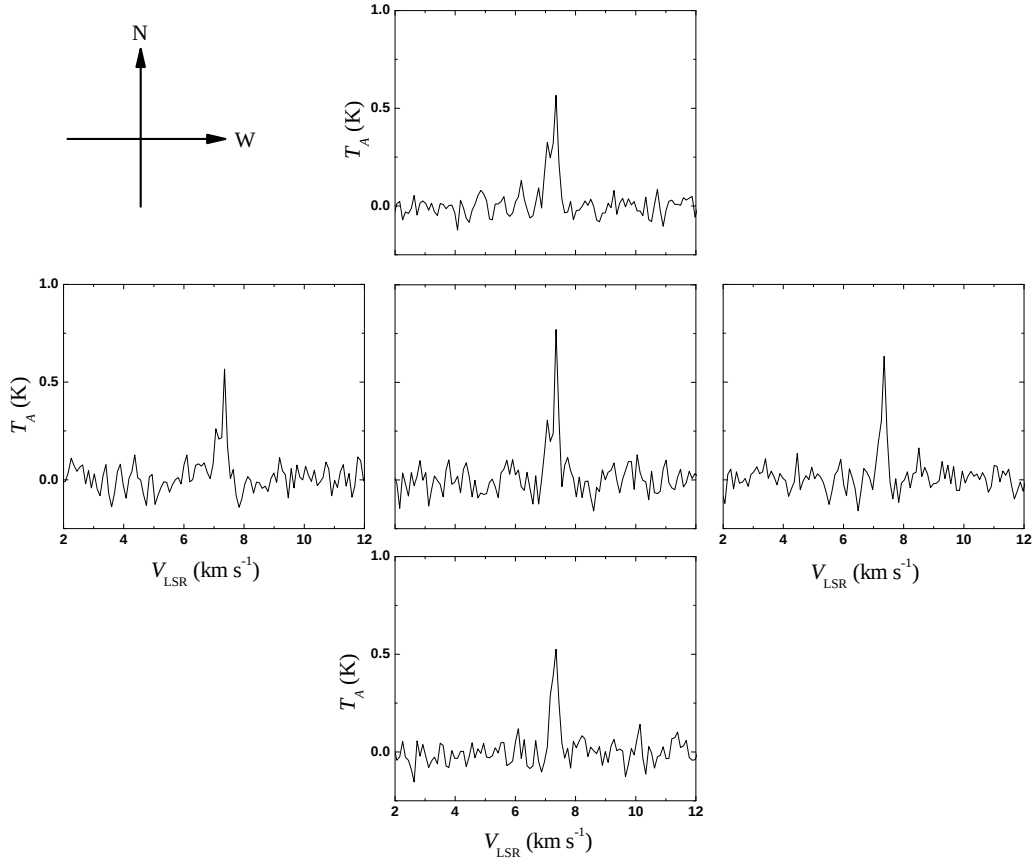

Figure D.1: Five-point map of C_4H around the N_2D^+ peak position in L1544. The grid spacing is approximately 30″.

Appendix E

Estimates of Fractional Ionization from Molecular Anions

Molecular anions may provide an independent means of estimating the fractional ionization ($x_e \equiv e/\mathrm{H}_2$) of molecular clouds (see, e.g., ref. [149]). So far, x_e has mainly been estimated indirectly from observations of molecular cations in conjunction with chemical models, and large uncertainties remain in its determination (for a review, see ref. [159]). The most reliable estimate of x_e might be obtained from a simultaneous analysis of the measured abundances of anions and cations based on the assumption that they are codisributed in the cloud.

The formation of $\mathrm{C_6H^-}$ likely occurs *via* radiative attachment

$$\mathrm{C_6H} + e \xrightarrow{k_{ra}} \mathrm{C_6H^-} + h\nu, \tag{E.1}$$

and its destruction by neutralization with positive ions and associative detachment with atomic hydrogen

$$\mathrm{C_6H^-} + \mathrm{M^+} \xrightarrow{k_{neu}} \mathrm{C_6H} + \mathrm{M}, \tag{E.2}$$

$$\mathrm{C_6H^-} + \mathrm{H} \xrightarrow{k_{ad}} \mathrm{HC_6H} + e, \tag{E.3}$$

where M^+ is any positive ion. We neglect the formation of C_6H^- by dissociative attachment to C_6H_2 (carbene) and HC_6H (triacetylene): C_6H_2 has not been observed in L1544 and L1521F, whereas dissociative attachment to HC_6H is endothermic by about 160 kJ mol^{-1} and hence unfavorable [99]. We also neglect the destruction of C_6H^- by charge transfer to large molecules or grains and by photodetachment; charge transfer is nearly six orders of magnitude and photodetachment more than one order of magnitude slower than the reactions (A2) and (A3) (see, e.g., ref. [97, 99]). At steady state,

$$\frac{[C_6H^-]}{[C_6H]} = \frac{k_{ra}[e]}{(k_{neu}[M^+] + k_{ad}[H])}, \tag{E.4}$$

where $[e]$ is the abundance of electrons, $[M^+]$ that of cations, and [H] that of atomic hydrogen. We adopt $k_{ra} = 5 \times 10^{-8}$ cm^3s^{-1} obtained from observations toward two quite different sources (IRC+10216 and L1527; [96, 99]); $k_{ad} = 5 \times 10^{-10}$ cm^3s^{-1} was accurately determined from laboratory measurements [23]. On the assumption that reaction (A3) is the dominant loss mechanism of C_6H^- at densities $< 10^6$ cm^{-3} [99], equation (A4) reduces to

$$\frac{[C_6H^-]}{[C_6H]} \sim \frac{k_{ra}[e]}{k_{ad}[H]}. \tag{E.5}$$

In L1544 and L1521F, the gas densities are estimated to lie between $10^4 - 10^5$ cm^{-3} except in the dense cores [143, 144]. From A5, $[e]/[H]$ is 2.5×10^{-4} for L1544 and 4×10^{-4} for L1521F. Adopting $[H]/[H_2] = 1 \times 10^{-3}$ cm^{-3} [150], our estimate of $x_e = 10^{-8} - 10^{-7}$ is somewhat higher than that from earlier measurements of N_2D^+/N_2H^+ [143, 144], but close to that obtained from observations of CO, HCO^+, and DCO^+ in dense cores [126, 160].

Bibliography

[1] G. C. Reid, J. Geophys. Res. **13**, 2551 (1975).

[2] W. Grübler, W. Haeberli, and P. Schwandt, Phys. Rev. Lett. **12**, 595 (1964).

[3] R. Wildt, Astrophys. J. **89**, 295 (1939).

[4] R. Wildt, Astrophys. J. **90**, 611 (1939).

[5] D. R. Bates, Astrophys. J. **91**, 202 (1940).

[6] S. Chandrasekhar, Astrophys. J. **102**, 223 (1945).

[7] L. M. Branscombe and S. J. Smith, Phys. Rev. **98**, 1028 (1955).

[8] H. S. W. Massey, *Negative Ions*, Cambridge University Press, 1976.

[9] J. J. Thomson, Phil. Mag. **13**, 561 (1907).

[10] A. Dalgarno and R. A. McCray, Astrophys. J. **181**, 90 (1973).

[11] K. D. Tucker, M. L. Kutner, and P. Thaddeus, Astrophys. J. **193**, L115 (1974).

[12] M. Guélin and P. Thaddeus, Astrophys. J. **212**, L81 (1977).

[13] M. Guélin, S. Green, and P. Thaddeus, Astrophys. J. **224**, L27 (1978).

[14] P. J. Sarre, J. Chim. Phys. Phys.-Chim. Biol. **77**, 769 (1980).

[15] E. Herbst, Nature **289**, 656 (1981).

[16] S. R. Lepp and A. Dalgarno, Astrophys. J. **324**, 553 (1988).

[17] S. R. Lepp and A. Dalgarno, Astrophys. J. **335**, 769 (1988).

[18] G. H. Herbig, Annu. Rev. Astron. & Astrophys. **33**, 19 (1995).

[19] M. Tulej, D. A. Kirkwood, M. Pachkov, and J. P. Maier, Astrophys. J. **506**, L69 (1998).

[20] B. J. McCall, J. Thorburn, L. M. Hobbs, T. Oka, and D. York, Astrophys. J. **559**, L135 (2001).

[21] D. P. Ruffle, R. P. A. Bettens, R. Terzieva, and E. Herbst, Astrophys. J. **573**, 678 (1999).

[22] R. Terzieva and E. Herbst, Int. J. Mass. Spectrom. **201**, 135 (2000).

[23] C. Barckholtz, T. P. Snow, and V. M. Bierbaum, Astrophys. J. **547**, L171 (2001).

[24] S. J. Blanksby, A. M. McAnoy, S. Dua, and J. H. Bowie, Mon. Not. Roy. Astr. Soc. **328**, 89 (2001).

[25] S. Civiš et al., Publ. Astron. Soc. Japan **57**, 605 (2005).

[26] Y. Morisawa et al., Publ. Astron. Soc. Japan **57**, 325 (2005).

[27] H. Suzuki, M. Ohishi, N. Kaifu, S. Ishikawa, and T. Kasuga, Publ. Astron. Soc. Japan **38**, 911 (1986).

[28] M. Guélin, J. Cernicharo, C. Kahane, J. Gomez-Gonzalez, and C. M. Walmsley, Astron. & Astrophys. **175**, L5 (1987).

[29] K. Kawaguchi, Y. Kasai, S. Ishikawa, and N. Kaifu, Publ. Astron. Soc. Japan **47**, 853 (1995).

[30] J. Cernicharo, M. Guélin, M. Hein, and C. Kahane, Astron. & Astrophys. **181**, L9 (1986).

[31] M. Guélin and J. Cernicharo, Astron. & Astrophys. **309**, L27 (1996).

[32] J. C. Pearson, C. A. Gottlieb, D. R. Woodward, and P. Thaddeus, Astron. & Astrophys. **189**, L13 (1988).

[33] M. C. McCarthy, C. A. Gottlieb, H. Gupta, and P. Thaddeus, Astrophys. J. **652**, L141 (2006).

[34] H. Linnartz et al., J. Mol. Spect. **197**, 1 (1999).

[35] M. Fehér and J. P. Maier, Chem. Phys. Lett. **227**, 371 (1994).

[36] I. Shnitko et al., J. Phys. Chem. A **110**, 2885 (2006).

[37] K. Aoki, Chem. Phys. Lett. **323**, 55 (2000).

[38] M. Agúndez and J. Cernicharo, Astrophys. J. **650**, 374 (2006).

[39] S. Petrie, E. Kagi, and K. Kawaguchi, Mon. Not. R. Astron. Soc. **343**, 209 (2003).

[40] J. C. Rienstra-Kirakofe, G. S. Tschumper, H. F. Schaefer III, S. Nandi, and G. B. Ellison, Chem. Rev. **102**, 231 (2002).

[41] T. Amano, J. Chem. Phys. **129**, 244305 (2008).

[42] S. Civiš, A. Walters, M. Y. Tretyakov, S. Bailleaux, and M. Bogey, J. Chem. Phys. **108**, 8369 (1998).

[43] F. Matsushima, T. Yonezu, T. Okabe, K. Tomaru, and Y. Moriwaki, J. Mol. Spec. **235**, 261 (2006).

[44] H. Gupta, C. A. Gottlieb, M. C. McCarthy, and P. Thaddeus, Astrophys. J. **691**, 1494 (2009).

[45] T. D. Crawford and H. F. Schaefer III, Rev. Comp. Chem. **14**, 33 (2000).

[46] K. Raghavachari, G. W. Trucks, J. A. Pople, and M. Head-Gordon, Chem. Phys. Lett. **157**, 479 (1989).

[47] P. Botschwina, M. Horn, K. Markey, and R. Oswald, Mol. Phys. **92**, 381 (1997).

[48] P. Botschwina and M. Horn, J. Mol. Spec. **185**, 191 (1997).

[49] P. Botschwina, Mol. Phys. **103**, 1441 (2005).

[50] J. Gauss and J. F. Stanton, Chem. Phys. Lett. **276**, 70 (1997).

[51] M. J. Travers, M. C. McCarthy, C. A. Gottlieb, and P. Thaddeus, Astrophys. J. **483**, L135 (1997).

[52] M. C. McCarthy et al., J. Chem. Phys. **111**, 6750 (1999).

[53] K. W. Sattelmeyer and J. F. Stanton, J. American Chem. Soc **122**, 8220 (2000).

[54] M. C. McCarthy and P. Thaddeus, Astrophys. J. **569**, L55 (2002).

[55] J. Cernicharo, M. Guélin, M. Agúndez, M. C. McCarthy, and P. Thaddeus, Astrophys. J. **688**, L83 (2008).

[56] P. Botschwina and R. Oswald, J. Mol. Spec. **254**, 47 (2009).

[57] T. H. Dunning, J. Chem. Phys. **90**, 1007 (1989).

[58] D. E. Woon and T. H. Dunning, J. Chem. Phys. **98**, 1358 (1993).

[59] A. K. Wilson, T. van Mourik, and T. H. Dunning, J. Mol. Struct. **388**, 339 (1996).

[60] A. K. Wilson, D. E. Woon, K. A. Peterson, and T. H. Dunning, J. Chem. Phys. **110**, 76677 (1999).

[61] T. van Mourik and T. H. Dunning, Int. J. Quantum Chem. **76**, 205 (2000).

[62] J. F. Stanton, J. Gauss, W. J. Lauderdale, and R. J. Bartlett, Int. J. Quantum Chem. Symp. **26**, 879 (1992).

[63] J. F. Stanton et al., ACES II Mainz-Austin-Budapest version, 2005-2008, see http://www.aces2.de.

[64] J. F. Stanton and J. Gauss, Int. Rev. Phys. Chem. **19**, 61 (2000).

[65] I. M. Mills, in *Modern Spectroscopy: Modern Research*, edited by K. N. Rao and C. W. Matthews, Academic Press, New York, 1972, p. 115.

[66] A. L. L. East, C. Johnson, and W. Allen, J. Chem. Phys. **98**, 1299 (1993).

[67] F. Pawlowski et al., J. Chem. Phys. **116**, 6482 (2002).

[68] P. Pyykkö, Mol. Phys. **106**, 1965 (2008).

[69] M. Mladenovic, P. Botschwina, P. Sebald, and S. Carter, Theor. Chem. Acc. **100**, 134 (1998).

[70] P. Botschwina and R. Oswald, Int. J. Mass Spect. **277**, 180 (2008).

[71] P. Botschwina and R. Oswald, J. Chem. Phys. **129**, 044305 (2008).

[72] T. J. Lee and C. E. Dateo, Spectrochim. Acta. A **55**, 739 (1999).

[73] H. Spahn et al., Chem. Phys. **346**, 132 (2008).

[74] R. Polák and J. Fišěr, Spectrochim. Acta A **58**, 2029 (2002).

[75] H. Gupta et al., Astrophys. J. **655**, L57 (2007).

[76] S. Brünken, H. Gupta, C. A. Gottlieb, M. C. McCarthy, and P. Thaddeus, Astrophys. J. **664**, L43 (2007).

[77] C. A. Gottlieb, S. Brünken, M. C. McCarthy, and P. Thaddeus, J. Chem. Phys. **126**, 191101 (2007).

[78] P. Thaddeus et al., Astrophys. J. **677**, 1132 (2008).

[79] S. Brünken, C. A. Gottlieb, H. Gupta, M. C. McCarthy, and P. Thaddeus, Astron. & Astrophys. **464**, L33 (2007).

[80] C. A. Gottlieb, P. C. Myers, and P. Thaddeus, Astrophys. J. **588**, 655 (2003).

[81] R. Mollaaghababa, C. A. Gottlieb, and P. Thaddeus, J. Chem. Phys. **98**, 968 (1993).

[82] S. K. Stephenson and R. J. Saykally, Chem. Rev. **105**, 3220 (2005).

[83] M. C. McCarthy, W. Chen, M. J. Travers, and P. Thaddeus, Astrophys. J. Suppl. **129**, 611 (2000).

[84] T. R. Taylor, C. Xu, and D. M. Neumark, J. Chem. Phys. **108**, 10018 (1998).

[85] M. C. McCarthy and P. Thaddeus, J. Chem. Phys. **129**, 054314 (2008).

[86] W. Gordy and R. L. Cook, *Microwave Molecular Spectra*, Wiley (Interscience), New York, 1984.

[87] C. A. Gottlieb, E. W. Gottlieb, P. Thaddeus, and H. Kawamura, Astrophys. J. **275**, 916 (1983).

[88] K. Graupner, T. L. Merrigan, T. A. Field, T. G. A. Youngs, and P. Marr, New. J. Phys. **8**, 117 (2006).

[89] P. Thaddeus, M. C. McCarthy, M. J. Travers, C. A. Gottlieb, and W. Chen, Faraday Discuss. **109**, 121 (1998).

[90] T. J. Millar, C. Walsh, M. A. Cordiner, R. Ni-Chuimin, and E. Herbst, Astrophys. J. **662**, L87 (2007).

[91] M. C. McCarthy, C. A. Gottlieb, P. Thaddeus, M. Horn, and P. Botschwina, J. Chem. Phys. **103**, 7820 (1995).

[92] T. Pino, M. Tulej, F. Güthe, M. Pachkov, and J. P. Maier, J. Chem. Phys. **116**, 6126 (2002).

[93] M. Pachkov et al., Mol. Phys. **101**, 583 (2003).

[94] A. L. Padellec et al., J. Chem. Phys. **115**, 10671 (2001).

[95] K. R. Lykke, D. M. Neumark, T. Andersen, V. J. Trapa, and W. C. Lineberger, J. Chem. Phys. **87**, 6842 (1987).

[96] J. Cernicharo et al., Astron. & Astrophys. **467**, L37 (2007).

[97] M. Agúndez et al., Astron. & Astrophys. **478**, L19 (2008).

[98] Y. Kasai, E. Kagi, and K. Kawaguchi, Astrophys. J. **661**, L61 (2007).

[99] N. Sakai, T. Sakai, Y. Osamura, and S. Yamamoto, Astrophys. J. **667**, L65 (2007).

[100] K. Kawaguchi et al., Publ. Astron. Soc. Japan **59**, L47 (2007).

[101] A. J. Remijan et al., Astrophys. J. **664**, L47 (2007).

[102] K. Rohlfs and T. L. Wilson, *Tools of Radio Astronomy*, Astronomy & Astrophysics Library, Springer-Verlag, 4th edition, 2004.

[103] S. E. Cummins, R. A. Linke, and P. Thaddeus, Astrophys. J. Suppl. **60**, 819 (1986).

[104] M. B. Bell et al., Astrophys. J. **518**, 740 (1999).

[105] M. C. McCarthy, W. Chen, A. J. Apponi, C. A. Gottlieb, and P. Thaddeus, Astrophys. J. **520**, 158 (1999).

[106] W. Chen, S. E. Novick, M. C. McCarthy, C. A. Gottlieb, and P. Thaddeus, J. Chem. Phys. **103**, 7828 (1995).

[107] K. R. Lykke, R. D. Mead, and W. C. Lineberger, Phys. Rev. Lett. **52**, 2221 (1984).

[108] F. Güthe, M. Tulej, M. Pachkov, and J. P. Maier, Astrophys. J. **555**, 466 (2001).

[109] C. Desfrancois, H. Abdoul-Carime, and J.-P. Schermann, Int. J. Mod. Phys. **116**, 6126 (1996).

[110] D. E. Woon, Chem. Phys. Lett. **244**, 45 (1995).

[111] M. C. McCarthy, M. J. Travers, A. Kovàcs, C. A. Gottlieb, and P. Thaddeus, Astron. & Astrophys. **309**, L31 (1996).

[112] W. M. Irvine et al., Astrophys. J. **334**, L107 (1988).

[113] S. Petrie and E. Herbst, Astrophys. J. **491**, 210 (1997).

[114] A. E. Douglas and G. Herzberg, Astrophys. J. **94**, 381 (1941).

[115] B. E. Turner and P. Thaddeus, Astrophys. J. **211**, 755 (1977).

[116] M. Womack, L. M. Ziurys, and S. Wyckoff, Astrophys. J. **387**, 417 (1992).

[117] P. Caselli, P. J. Benson, P. C. Myers, and M. Tafalla, Astrophys. J. **572**, 238 (2002).

[118] E. Herbst and Y. Osamura, Astrophys. J. **679**, 1670 (2008).

[119] R. Bachiller, K. M. Menten, and S. del Río-Alvarez, Astron. & Astrophys. **236**, 461 (1990).

[120] T. Hirota, H. Maezawa, and S. Yamamoto, Astrophys. J. **617**, 399 (2004).

[121] A. Belloche, P. André, D. Despois, and S. Blinder, Astron. & Astrophys. **393**, 927 (2002).

[122] A. Crapsi et al., Astrophys. J. **619**, 379 (2005).

[123] T. Hirota, T. Ito, and S. Yamamoto, Astrophys. J. **565**, 359 (2002).

[124] N. Sakai, T. Sakai, T. Hirota, and S. Yamamoto, Astrophys. J. **672**, 371 (2008).

[125] G. A. Fuller and P. C. Myers, Astrophys. J. **418**, 273 (1993).

[126] J. P. Williams, E. A. Bergin, P. Caselli, P. C. Myers, and R. Plume, Astrophys. J. **503**, 689 (1998).

[127] B. E. Turner, Astrophys. J. **420**, 661 (1994).

[128] J. V. Buckle et al., Faraday Discuss. **133**, 63 (2006).

[129] P. Cox, R. Güsten, and C. Henkel, Astron. & Astrophys. **206**, 108 (1988).

[130] R. Lucas and H. S. Liszt, Astron. & Astrophys. **358**, 1069 (2000).

[131] D. Teyssier et al., Astron. & Astrophys. **417**, 135 (2004).

[132] B. Lefloch, A. Castets, J. Cernicharo, W. D. Langer, and R. Zylka, Astron. & Astrophys. **334**, 269 (1998).

[133] J. K. Jörgensen et al., Astrophys. J. **632**, 973 (2005).

[134] M. Morris, B. E. Turner, P. Palmer, and B. Zuckerman, Astrophys. J. **205**, 82 (1976).

[135] S. C. Madden, W. M. Irvine, H. Matthew, P. Friberg, and D. A. Swade, Astron. J. **97**, 1403 (1989).

[136] S. Fukasaku et al., Astrophys. J. **437**, 410 (1994).

[137] J. L. Highberger, C. Savage, J. H. Bieging, and L. M. Ziurys, Astrophys. J. **562**, 790 (2001).

[138] J. L. Highberger, K. J. Thomson, P. A. Young, D. Arnett, and L. M. Ziurys, Astrophys. J. **593**, 393 (2003).

[139] T. L. Bourke et al., Astrophys. J. **649**, L37 (2006).

[140] M. Tafalla et al., Astrophys. J. **504**, 900 (1998).

[141] N. Ohashi, S. Lee, D. J. Wilner, and M. Hayashi, Astrophys. J. **518**, L41 (1999).

[142] P. Caselli, C. M. Walmsley, A. Zucconi, M. Tafalla, and P. C. Myers, Astrophys. J. **565**, 331 (2002).

[143] P. Caselli, C. M. Walmsley, A. Zucconi, M. Tafalla, and P. C. Myers, Astrophys. J. **565**, 344 (2002).

[144] A. Crapsi et al., Astron. & Astrophys. **420**, 957 (2004).

[145] C. Codella, R. Welser, C. Henkel, P. J. Benson, and P. C. Myers, Astron. & Astrophys. **324**, 203 (1997).

[146] S. R. Federman, W. T. Huntress, and S. S. Prasad, Astrophys. J. **354**, 504 (1990).

[147] G. F. Mitchell and W. T. Huntress, Nature **278**, 722 (1979).

[148] H. I. Schiff and D. K. Bohme, Astrophys. J. **252**, 740 (1979).

[149] D. R. Flower, G. P. des Forêts, and C. M. Walmsley, Astron. & Astrophys. **474**, 923 (2007).

[150] D. Li and P. F. Goldsmith, Astrophys. J. **585**, 823 (2003).

[151] P. F. Goldsmith, D. Li, and M. Krco, Astrophys. J. **654**, 273 (2007).

[152] N. Sakai, T. Sakai, T. Hirota, M. Burton, and S. Yamamoto, Astrophys. J. **697**, 769 (2009).

[153] T. Hirota and S. Yamamoto, Astrophys. J. **646**, 258 (2006).

[154] L. A. Nyman et al., Astron. & Astrophys. **269**, 377 (1993).

[155] E. Herbst and W. Klemperer, Astrophys. J. **185**, 505 (1973).

[156] T. R. Geballe and T. Oka, Nature **384**, 334 (1996).

[157] F. A. Miller and D. H. Lemon, Spectrochim. Acta A **23**, 1415 (1967).

[158] W. Dannhauser and A. F. Flueckinger, J. Chem. Phys. **38**, 69 (1963).

[159] P. Caselli, Planet. Space Sci. **50**, 1133 (2002).

[160] P. Caselli, C. M. Walmsley, R. Terzieva, and E. Herbst, Astrophys. J. **499**, 234 (1998).

Vita

Harshal Dilip Gupta was born in Nagpur, India on 28 February 1980 to Mandakini and Dilip Gupta. He received his secondary school certificate from Bhavan's Vidya Mandir, Nagpur, in 1998, and a Bachelor of Science in Chemistry from the University of Texas at Austin in 2003. He began graduate study at the Department of Chemistry and Biochemistry at UT Austin in 2003. From 2005 through 2008, he was a visiting student at the School of Engineering and Applied Sciences, Harvard University, and at the Smithsonian Astrophysical Observatory in Cambridge, MA. He completed his doctoral work in Chemical Physics at UT Austin in 2009, and accepted a position at the California Insitute of Technology, Pasadena, CA, working as a post-doctoral scholar at the Jet Propulsion Laboratory.

Permanent address: 1209 Red Ranch Circle
Cedar Park, TX 78613

This dissertation was typeset with LaTeX[†] by the author.

[†]LaTeX is a document preparation system developed by Leslie Lamport as a special version of Donald Knuth's TeX Program.